JOURNAL OF PETROLOGY | VOLUME 42 | NUMBER 3 | PAGES 459–486 | 2001

Magmatic Evolution of the La Pacana Caldera System, Central Andes, Chile: Compositional Variation of Two Cogenetic, Large-Volume Felsic Ignimbrites

J. M. LINDSAY[1]*, A. K. SCHMITT[1], R. B. TRUMBULL[1], S. L. DE SILVA[2], W. SIEBEL[1]‡ AND R. EMMERMANN[1]

[1]GEOFORSCHUNGSZENTRUM POTSDAM, TELEGRAFENBERG, 14473 POTSDAM, GERMANY

[2]INDIANA STATE UNIVERSITY, TERRE HAUTE, IN 47089, USA

RECEIVED NOVEMBER 18, 1999; REVISED TYPESCRIPT ACCEPTED JUNE 2, 2000

La Pacana is one of the largest known calderas on Earth, and is the source of at least two major ignimbrite eruptions with a combined volume of some 2700 km^3. These ignimbrites have strongly contrasting compositions, raising the question of whether they are genetically related. The Toconao ignimbrite is crystal poor, and contains rhyolitic (76–77 wt % SiO_2) tube pumices. The overlying Atana ignimbrite is a homogeneous tuff whose pumice is dacitic (66–70 wt % SiO_2), dense (40–60% vesicularity) and crystal rich (30–40% crystals). Phase equilibria indicate that the Atana magma equilibrated at temperatures of 770–790°C with melt water contents of 3·1–4·4 wt %. The pre-eruptive Toconao magma was cooler (730–750°C) and its melt more water rich (6·3–6·8 wt % H_2O). A pressure of 200 MPa is inferred from mineral barometry for the Atana magma chamber. Isotope compositions are variable but overlapping for both units ($^{87}Sr/^{86}Sr_i$ 0·7094–0·7131; $^{143}Nd/^{144}Nd$ 0·51222–0·51230) and are consistent with a dominantly crustal origin. Glass analyses from Atana pumices are similar in composition to those in Toconao tube pumices, demonstrating that the Toconao magma could represent a differentiated melt of the Atana magma. Fractional crystallization modelling suggests that the Toconao magma can be produced by 30% crystallization of the observed Atana mineral phases. Toconao melt characteristics and intensive parameters are consistent with a volatile oversaturation-driven eruption. However, the low H_2O content, high viscosity and high crystal content of the Atana magma imply an external eruption trigger.

KEY WORDS: *Central Andes; crystal-rich dacite; eruption trigger; high-silica rhyolite; zoned magma chamber*

INTRODUCTION

The study of large silicic caldera systems addresses some of the most intriguing problems in igneous petrology and volcanology. First, the crystal-rich dacitic ignimbrites commonly erupted from these systems present snapshots of the processes taking place within large magma chambers, thus providing an instantaneous record that cannot be studied in slowly cooled plutonic bodies. The development of magma chamber zonation, for example, has been approached through the study of ignimbrites by several workers since the studies of Smith (1960) and Smith & Bailey (1966), and this has led to the general thesis that these large homogeneous dacitic ignimbrites appear to erupt from magma chambers that were unzoned or only weakly zoned (e.g. Whitney & Stormer, 1985; Francis *et al.*, 1989; de Silva, 1991). Second, the origin of the huge volumes of felsic magmas represented by these large caldera systems remains enigmatic. Some examples are thought to have dominantly mantle-derived sources (e.g. Smith *et al.*, 1996). In other cases, crustal anatexis is favoured as a dominant process although questions remain as to the contribution of mantle-derived melts and the importance of differentiation processes in upper-crustal magma chambers (e.g. Whitney & Stormer, 1985; de Silva, 1989*a*; Francis *et al.*, 1989; Ort *et al.*, 1996). Finally, the eruption triggering of large dacitic ignimbrites is also poorly understood. Their high crystal contents and viscosities and the relatively low magma

*Corresponding author. Present address: Seismic Research Unit, University of the West Indies, St Augustine, Trinidad. Telephone: 001-868-662-4659. Fax: 001-868-662-9293. E-mail: sruuwi@tstt.net.tt

‡Present address: Lehrstuhl für Geochemie, Universität Tübingen, 72077 Tübingen, Germany.

Extended dataset can be found at: http://www.petrology.oupjournals.org

H_2O contents imply that the magmas may not be able to generate the critical overpressure for eruption through volatile exsolution alone (e.g. Scaillet *et al.*, 1998). Studies on old uplifted and eroded calderas whose roots are exposed (e.g. Kokelaar, 1992; Branney & Kokelaar, 1994; Moore & Kokelaar, 1998), together with the complexity and large size of many relatively young calderas and the great volumes of their associated ignimbrites, raise the question of how large ignimbrite eruptions may relate to extensional stress.

Some of the largest and best exposed examples of large-volume, intermediate-composition ignimbrites occur in the Central Andes of South America, where, during the Late Tertiary to Recent, explosive eruptions produced one of the most extensive ignimbrite provinces of the world (Guest, 1969; Pichler & Zeil, 1972; de Silva, 1989*a*). The calderas and ignimbrites of this province are typically located $\leq$200 km east of the modern arc in the arid Altiplano–Puna Plateau, the highest plateau in the world associated with abundant arc magmatism. Also particular to this region is the exceptionally thick crust: refraction experiments (Wigger *et al.*, 1994) and broadband passive seismology suggest thicknesses of 70–80 km (Zandt *et al.*, 1994; Beck *et al.*, 1996). The largest concentration of Neogene ignimbrites in the Central Andes has been designated by de Silva (1989*a*) as the Altiplano–Puna Volcanic Complex (APVC) (Fig. 1). Located between $\sim$21°S and 24°S, the APVC covers some 70 000 km^2 and represents >30 000 km^3 of late-Miocene to Pleistocene crystal-rich, dacitic ignimbrites (e.g. de Silva & Francis, 1989). The young age, excellent preservation and particular regional tectonic setting of the APVC make it a compelling focus for studies of large-volume ignimbrites. Recently, a zone of extremely low S-wave velocities and high electrical conductivity has been recognized at $\sim$20 km depth beneath the APVC, and explained by the presence of at least 10–20 vol. % partial melt residing in the crust (Schilling *et al.*, 1997; Schmitz *et al.*, 1997). This zone, which lies in the crust beneath this major ignimbrite province, has been described as possibly the largest known near-molten magma body on Earth (Chmielowski *et al.*, 1999).

La Pacana caldera, 60 km $\times$ 35 km in size, is the largest of the APVC centres (Gardeweg & Ramírez, 1987). It is the source of at least two major, compositionally different, but effectively coeval ignimbrites: the rhyolitic Toconao ignimbrite and the overlying, dacitic Atana ignimbrite (Lindsay, 1999). This paper presents the first detailed petrological, geochemical and isotopic study of these ignimbrites. A companion paper (Lindsay *et al.*, 2001) describes the geology of the La Pacana caldera in detail. The present study sheds light on some of the main issues related to large-volume silicic systems described above. Evidence is given that the two ignimbrites are cogenetic and erupted from a strongly zoned magma chamber. The source of the common parental magma is considered to be dominantly crustal. The study furthermore permits an evaluation of the eruption triggers of these contrasting ignimbrites.

GEOLOGY OF LA PACANA CALDERA

Activity associated with La Pacana caldera began in the early Pliocene with the eruption of the $\sim$5 Ma rhyolitic Toconao ignimbrite (Lindsay *et al.*, 2001). This was followed by the main caldera-forming event, which produced the dacitic Atana ignimbrite (Fig. 2). Post-eruption resurgence of the Atana magma led to the formation of an elongate block of intracaldera tuff known as the Cordón La Pacana, and post-caldera volcanism produced several small silicic domes along the margin of the resurgent block and within the moat (Fig. 2). Not all of these post-caldera domes have been dated, but available K–Ar age dates show that extrusive magmatism continued from 4·1 Ma until at least 1·6 Ma (Lindsay *et al.*, 2001). These centres are dominantly crystal-rich dacite with mineral assemblages and geochemical characteristics similar to the Atana pumices, and are thought to represent late-erupted, degassed portions of the Atana magma (Lindsay, 1999).

The Toconao ignimbrite is a crystal-poor, moderately lithic-rich, rhyolitic ignimbrite with an estimated outflow volume of 180 km^3 (Lindsay *et al.*, 2001). Available K–Ar dates range between 4·0 $\pm$ 0·9 and 5·3 $\pm$ 1·1 Ma (Gardeweg & Ramírez, 1987; de Silva, 1989*b*; Lindsay *et al.*, 2001). The Toconao ignimbrite comprises two main facies (Fig. 3): a lower, non-welded and non-indurated facies with abundant distinctive tube pumices, and an upper facies, which has been indurated by vapour-phase alteration. Locally, there is a thin (<10 cm) plinian airfall deposit at the base, which contains small, aphyric tube pumices.

The Atana ignimbrite is a crystal-rich, homogeneous dacitic ignimbrite comprising an intracaldera and outflow facies with a combined estimated volume of 2500 km^3 (Lindsay *et al.*, 2001). K–Ar ages of pumices from this unit range from 3·8 $\pm$ 0·1 to 4·2 $\pm$ 0·1 Ma (Lindsay *et al.*, 2001). The intracaldera facies of the resurgent block is characterized by densely welded and devitrified tuffs. The Atana outflow typically occurs as a single flow unit $\sim$30–40 m thick, which locally is underlain by a surge deposit and a soft ash and pumice-rich layer (Fig. 3). The homogeneous, crystal-rich Atana tuff is generally moderately to strongly welded and shows various degrees of devitrification. It is poor in lithic fragments, and also relatively pumice poor.

Geological evidence for a hiatus between the erution of the Toconao ignimbrite and the overlying Atana ignimbrite is lacking. However, given the arid climate of

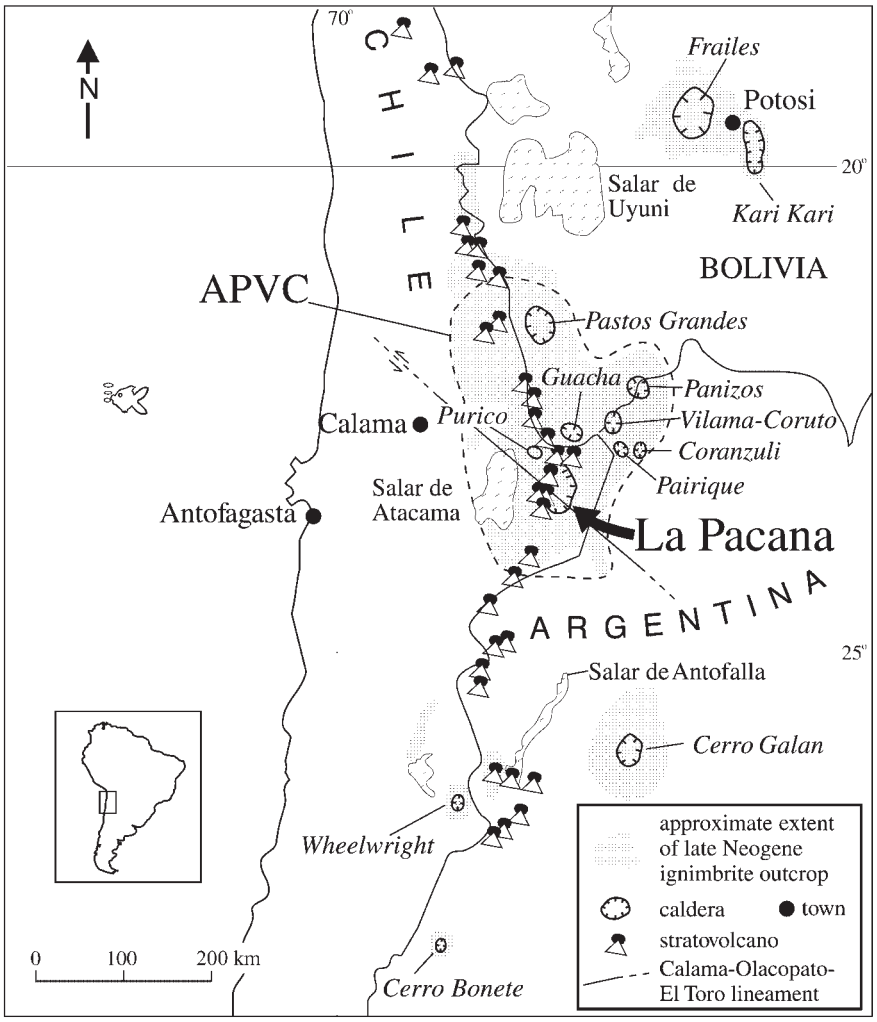

Fig. 1. Sketch map of part of the Central Andes showing the approximate extent of ignimbrite outcrop, the Altiplano–Puna Volcanic Complex (APVC) and location of main calderas. Location of the Calama–Olacopato–El Toro lineament after Salfity (1985).

the region and the inefficiency of erosion, a considerable hiatus could go unnoticed. The K–Ar age dating of the two ignimbrites is of insufficient precision to constrain the repose time between eruptions.

ANALYTICAL TECHNIQUES

Mineral compositions were determined on a Cameca SX100 electron microprobe equipped with four wavelength-dispersive spectrometers. Data reduction followed the PAP-correction scheme (Pouchou & Pichoir, 1984). An accelerating voltage of 15 kV was used, beam currents were generally between 10 and 20 nA, and beam diameter ranged from 2 to 20 μm. Analytical errors for major components (>10 wt %) are considered to be 1–2% (rel.), and for minor components (1–10 wt %) 3–10% (rel.). Qualitative analysis of mineral separates was carried out with a scanning electron microscope equipped with an energy dispersive spectrometer (EDS-SEM).

All geochemical and isotopic analyses were performed on fresh pumice samples. An effort was made to analyse single pumice clasts >5 cm in diameter; where necessary, however, several pumices from the same sample were prepared and analysed together. Whole-rock major elements and Ba, Cr, Rb, Sr, V, Y, Zn, Zr and Nb were determined by X-ray fluorescence spectrometry (Philips PW 2400 and Siemens SRS 303 AS with Rh tubes) on fused glass discs and pressed powder briquettes. Rare earth elements (REE) from representative samples were determined by inductively coupled plasma atomic emission spectrometry (ICP-AES) on a Varian Liberty 200 (Zuleger & Erzinger, 1988) and Th, U, Pb, Li, Cs and Ta from representative samples by inductively coupled plasma mass spectrometry (ICP-MS) using a VG Plasma

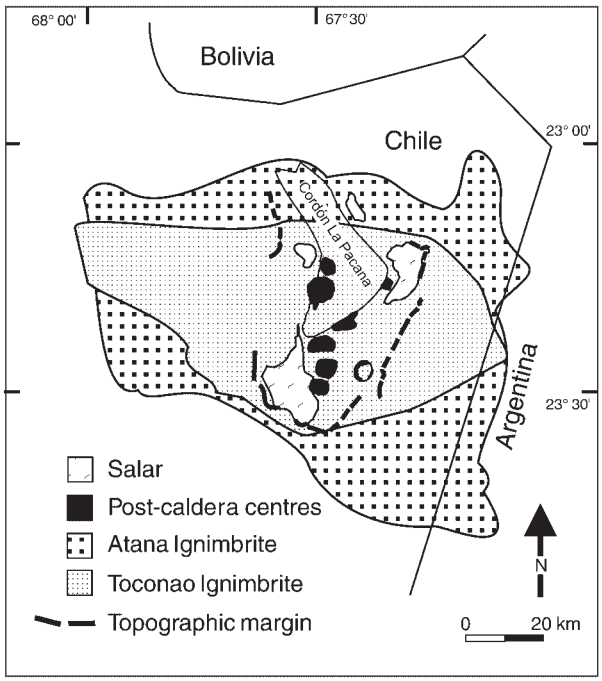

Fig. 2. Map showing the inferred distribution of the Toconao and Atana ignimbrites based on a line connecting their most distal known outcrops. (Note that this is not a geological map.) Except to the extreme west of the study area where it outcrops at the surface, the Toconao ignimbrite is covered both within the caldera and in the outflow sheets by the Atana ignimbrite (see Fig. 3) and only crops out in valleys and in the caldera wall. The locations of post-caldera centres are shown in black.

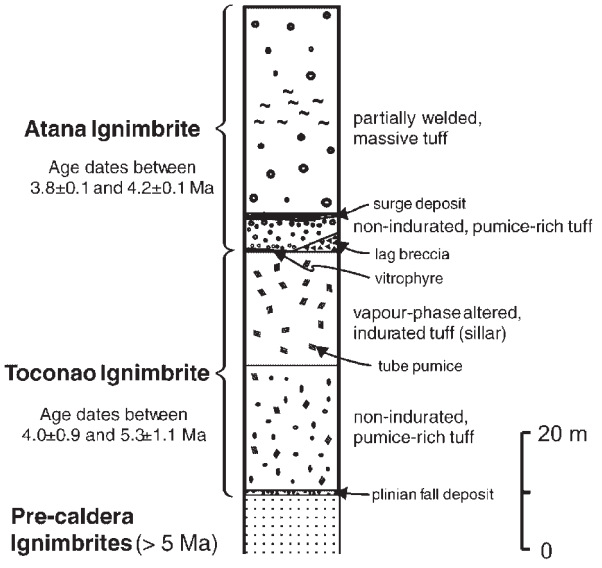

Fig. 3. Generalized stratigraphic section and ages of the La Pacana ignimbrites (extracaldera).

Quad PQ^{2+}. H_2O and CO_2 were analysed after thermal extraction by IR spectroscopy using an automated LECO RC-412 spectrometer. Analytical precision was better than $\pm 3\%$ (rel.) for all major elements, and considered to lie at $\pm 10\%$ (rel.) for trace elements. Relative error for REE analysis is considered to be <5%.

All isotopic analyses were carried out on unspiked whole-rock powders. Samples were dissolved by conventional digestion methods and Pb, Sr and Nd were separated using standard anion (Pb) and cation (Sr, Nd) exchange techniques [exchange resins for Pb: Bio Rad AG1-X8, 100–200 mesh; Sr, Nd: Bio Rad AW 50 W-X8, 100–200 mesh; Nd: di(2-ethylhexyl)-orthophosphoric acid (HDEHP)-coated Teflon powder]. Isotope ratios were determined on a Finnigan MAT 262 multicollector mass spectrometer (equipped with Faraday collectors) operating in static mode. Pb composition was measured on single Re filaments using a silica gel–H_3PO_4 emitter (Gerstenberger & Haase, 1997). A factor of 1·1‰ per mass unit Pb for instrumental mass fractionation was applied to all Pb analyses, using NBS SRM 981 as a reference standard. Sr and Nd samples were loaded on Ta filaments, and analysed using the single-filament mode for Sr and double-filament mode for Nd. In-run precision ($2\sigma_m$) of the $^{87}Sr/^{86}Sr$ and $^{143}Nd/^{144}Nd$ ratios is <0·002%. The $^{87}Sr/^{86}Sr$ ratios were normalized to $^{86}Sr/^{88}Sr = 0{\cdot}1194$ and the $^{143}Nd/^{144}Nd$ ratios to $^{146}Nd/^{144}Nd = 0{\cdot}7219$. Repeated analyses of the NBS 987 Sr standard and the La Jolla Nd standard gave average values of 0·710266 and 0·511910, respectively, and the measured $^{87}Sr/^{86}Sr$ and $^{143}Nd/^{144}Nd$ ratios were further adjusted to the NBS 987 reference value of 0·710248 and to the La Jolla reference value of 0·511858. Total procedural blanks were 30–50 pg for Pb, 100–200 pg for Sr and <50 pg for Nd.

Major element analyses of melt inclusions in quartz and matrix glass separates were determined by electron microprobe analysis (Cameca SX100). Melt inclusions were generally devitrified, and had to be heated for rehomogenization in a pressurized gas vessel using Ar as a pressure medium. Crystals were placed in an Au capsule, pressurized and then heated by a graphite furnace. Run conditions of heating were 800°C and 500 MPa for 24 h. The quenching rate was ~10°C/s. After heating, melt inclusions generally appeared transparent, homogeneous and without bubbles. Crystals with homogeneous inclusions were mounted in Araldite epoxy and polished to expose the inclusions. A 20 μm rastered beam and a 10 nA current were used in electron microprobe analysis to prevent Na diffusion.

Trace element compositions of glass were determined by secondary ion mass spectrometry (SIMS) on a modified CAMECA 3F at Arizona State University. A 1 nA ^{16}O primary beam with ~17 keV impact energy was focused on the sample surface to a spot diameter of ~20 μm.

The secondary column was set up for low mass resolution with entrance and exit slits wide open, a 150 μm field aperture and a 40 eV bandpass. Energy filtering to avoid molecular interferences was performed by applying a −75 V offset to the sample. Secondary ions were detected by an electron multiplier system. For quantification, $^{30}Si^{+}$ was analysed as a reference mass. NBS610 and NBS612 standard glasses were used for trace elements, and H_2O was calibrated on hydrous rhyolite glasses provided by H. Westrich, on which water concentrations were determined by Karl–Fischer titration (Westrich, 1987). Typical cumulative errors based on counting statistics for standards and samples are between 10 and 25% rel. (2σ) for trace element determination. The error in H_2O determination (0·3 wt % abs. 2σ) is mostly due to variations in the instrumental background signal.

PETROGRAPHY AND MINERAL CHEMISTRY

Typical tube pumices in the Toconao ignimbrite contain <1% crystals, comprising plagioclase, biotite, quartz, sanidine, hornblende, orthopyroxene, magnetite, ilmenite, zircon, apatite, monazite and minor epidote (Table 1). Many of the minor phases in the Toconao were identified by qualitative SEM-EDS analyses of heavy mineral separates from pumice (see Table 1) and their petrographic occurrence in the rock is unknown. Epidote is one of these, and it therefore cannot be said for sure if it is a primary phase. East of the caldera the Toconao tuff contains rounded crystal-poor (1–15% crystals) pumices that lack tubular texture in addition to the typical glassy tube pumices. These contain a similar mineral assemblage: plagioclase, sanidine, quartz and biotite (Table 1). Rare pumice types in the Toconao ignimbrite include small brown–white banded pumice and scoria.

Three types of pumices are distinguished in the Atana ignimbrite. The main type is crystal-rich pumice that contains 30–40% crystals comprising plagioclase, quartz, biotite, hornblende, minor sanidine and pyroxene, and accessory magnetite, titanite, ilmenite, zircon, apatite ± allanite (Table 1). The pumices range in size from a few centimetres to >30 cm and are relatively dense, with 40–60% vesicularity (Table 1).

At several localities the Atana ignimbrite also contains fine-grained, grey, crystal-rich (60–70% crystals) pumice inclusions that occur as individual clasts in the tuff or included in the crystal-rich pumices described above. The grey pumice inclusions have 40–50% vesicularity, and show no signs of textural disequilibrium with their host pumice clasts. They have a dominantly fine-grained matrix (<0·5 mm) of plagioclase, biotite, hornblende, clinopyroxene, minor orthopyroxene, and accessory magnetite, ilmenite, titanite, zircon and apatite (Table 1). Set within the fine-grained matrix are some large phenocrysts (>1 mm), similar to those of the host pumice. The overall percentage of ferromagnesian minerals in the grey pumice inclusions is fairly constant, but the bt:hbl:cpx ratio varies greatly (Table 1). Some samples display an ophimottled texture, and glomerocrysts of plagioclase and of hornblende + clinopyroxene are also present. Rare, crystal-poor (1–10% crystals) rhyolitic pumices constitute the third type of pumice in the Atana ignimbrite. These pumices typically occur in the non-indurated, crystal-poor basal zone of the ignimbrite (Fig. 2), and resemble the rounded, non-tubular crystal-poor pumices in the Toconao ignimbrite.

Mineral compositions determined by electron microprobe are summarized in Tables 2–5 and in Figs 4 and 5, and the main features of mineral petrography and composition are summarized briefly here. Plagioclase is the dominant feldspar and most abundant phenocryst in all Atana and Toconao pumice types. It is subhedral to anhedral, generally cracked, and exhibits a variety of zoning patterns. Plagioclase phenocrysts in Atana crystal-rich pumices and grey pumice inclusions have similar average core and rim compositions of $An_{38–49}$ and $An_{35–41}$, respectively (Fig. 4, Table 2). The rims are similar to microphenocryst compositions in the Atana pumice samples (An_{35}). Plagioclase in the crystal-poor Atana pumices is less calcic, with typical compositions of $An_{16–30}$ (core) and $An_{12–28}$ (rim). Unusually large plagioclase phenocrysts (up to 2 mm) in Atana crystal-rich pumices and grey pumice inclusions exhibit strong oscillatory zoning with rims of the same composition as those of the dominant plagioclase (An_{39}) but considerably more calcic cores ($An_{40–60}$ and $An_{53–84}$ in the pumices and grey pumice inclusions, respectively). Plagioclase in the Toconao ignimbrite is weakly zoned, with cores and rims within the range $An_{15–28}$ (average An_{22}), and occasionally more An-rich compositions between An_{33} and An_{49} (Fig. 4; Table 2). Sanidine is rare in the Atana pumice and tuff (<1%) but is present (up to 3%) in Toconao pumice and tuff. Sanidine is generally anhedral and somewhat rounded, with average compositions of $Ab_{25}Or_{74}An_1$ in the Atana and $Ab_{34}Or_{65}An_1$ in the Toconao pumice (Table 2). Sanidine locally forms rims around plagioclase grains. Such grains show no resorption of the plagioclase and the rims appear to be an overgrowth phenomenon.

Biotite is the most common ferromagnesian phase in all pumice types. It occurs as euhedral crystals up to 5 mm in diameter, commonly with inclusions of plagioclase, magnetite, apatite and zircon. Biotite crystals are typically bent or split and a few are embayed, but there are rarely signs of alteration. Zoning is weak or absent. Biotites in the Atana pumices and grey pumice inclusions have nearly constant compositions, with an *mg*-number of 0·55–0·60 (Table 3), whereas those in the Toconao pumices are slightly more magnesian (*mg*-number

Table 1: Modal analyses (dense rock equivalent, DRE) of Atana and Toconao pumices

Atana ignimbrite	Point counting					Mineral separates	
Sample:	Quis-96h-9 pumice	Lari-97h-4 pumice	Loy-97h-3 pumice	Lari-97h-6 gr. inclusion	Lari-96h-9 gr. inclusion	Atana pumice	gr. inclusion
Plagioclase (Pl)	18·7	18·2	23·1	42·4	35·2	x	x
Quartz (Qtz)	11·5	3·2	6·6	n.d.	n.d.	x	
Biotite (Bt)	5·9	3·5	5·8	14·8	4·7	x	x
Hornblende (Hbl)	1·7	0·3	1·7	5·9	16·3	x	x
Fe–Ti oxides (Mt, Ilm)	n.d.	0·9	1·4	1·3	2·4	x	x
Sanidine (Sa)	n.d.	0·2	n.d.	n.d.	n.d.	x	
Orthopyroxene (Opx)	n.d.	n.d.	0·2	0·3	0·2		x
Clinopyroxene (Cpx)	n.d.	n.d.	n.d.	2·9	0·1	x	x
Titanite (Ttn)	tr.	tr.	tr.	n.d.	n.d.	x	x
Zircon (Zrn)	tr.	tr.	tr.	tr.	tr.	x	x
Apatite (Ap)	tr.	tr.	tr.	tr.	tr.	x	x
Allanite (Aln)	n.d.	n.d.	n.d.	n.d.	n.d.	x	
Glass	62·2	73·8	61·4	32·6	41·1		
% crystals DRE	38	26	39	67	59		
% vesicularity	36	57	41	41	45		

Toconao ignimbrite	Point counting				Mineral separates	
Sample:	Quis-96h-21A x-poor pumice	Quis-96h-4A x-poor pumice	Toc-96h-2A tube pumice	Toc-96h-2B tube pumice	Toconao tube pumice	tuff
Plagioclase	9·5	7·8	n.d.	0·6	x	x
Quartz	2·6	0·8	n.d.	n.d.	x	x
Biotite	n.d.	0·8	1·0	0·6	x	x
Hornblende	n.d.	n.d.	n.d.	n.d.	x	x
Fe–Ti oxides	n.d.	n.d.	n.d.	n.d.	x	x
Sanidine	3·7	2·9	n.d.	n.d.	x	x
Orthopyroxene	n.d.	n.d.	n.d.	n.d.	x	x
Clinopyroxene	n.d.	n.d.	n.d.	n.d.		x
Zircon	n.d.	n.d.	n.d.	n.d.	x	x
Apatite	n.d.	n.d.	n.d.	n.d.	x	x
Monazite	n.d.	n.d.	n.d.	n.d.	x	x
Epidote	n.d.	n.d.	n.d.	n.d.	x	
Glass	84·1	87·7	99·0	98·8		
% crystals DRE	16	12	1	1		
% vesicularity	73	65	70	74		

Each analysis consisted of 1500–2500 point counts for Atana pumices (all from crystal-rich samples), and 400–1200 counts for Toconao pumices and Atana grey pumice inclusions. Grid size varied depending on grain size, but was commonly between 0·5 and 1 mm. n.d., not detected; tr., observed in trace amounts; x, present in mineral separate; % vesicularity is an estimate determined by density difference in air and water, following the method of Houghton & Wilson (1989).

0·59–0·64). Homogeneous, euhedral to subhedral amphibole crystals are subordinate to biotite in all pumice types. Compositionally, the amphiboles are mainly edenite and hornblende according to the nomenclature of Deer *et al.* (1992). Some compositions, particularly those from amphibole cores in grey pumice inclusions,

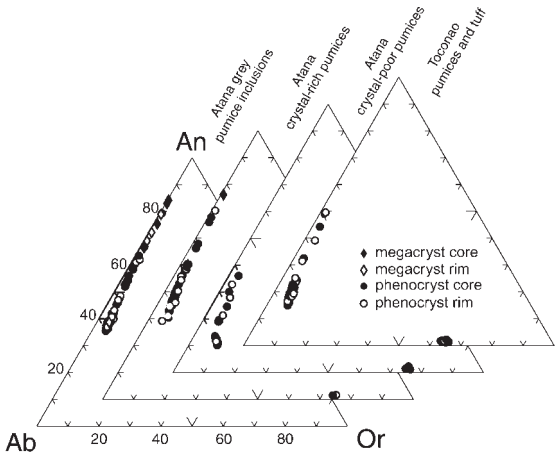

Fig. 4. Ab–An–Or ternary plot of feldspar compositions from the Atana and Toconao pumices.

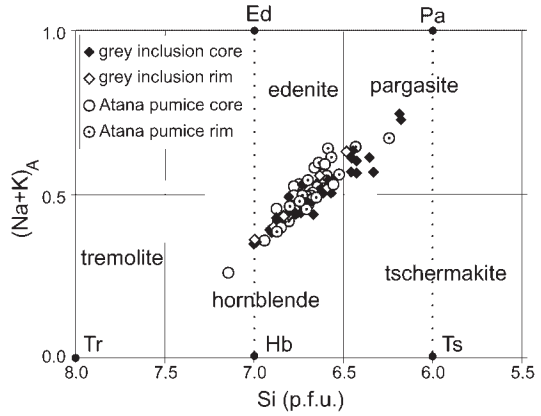

Fig. 5. Chemical variation of Atana amphiboles expressed as Na + K in A sites and Si atoms per formula unit. End members (marked as dots) are: Tr, tremolite; Hb, hornblende (*sensu stricto*); Ed, edenite; Pa, pargasite; Ts, tschermakite. Fields from Deer *et al.* (1992).

are pargasitic (Table 4; Fig. 5). The *mg*-number ranges from 0·53 to 0·71 in the grey pumice inclusions (average 0·62) and from 0·57 to 0·70 in the crystal-rich pumices (average 0·63) (Table 4). Magnetite (Atana: Usp_{14}; Toconao: Usp_{10}) and ilmenite (Atana: Hem_{29}; Toconao: Hem_{23}) are both present, and have no detectable exsolution or zoning (Table 5). Pink zircon and colourless apatite are common accessories in both the Atana and Toconao pumices, and yellow titanite is also present in Atana crystal-rich pumices and grey pumice inclusions.

WHOLE-ROCK GEOCHEMISTRY AND Pb-, Nd- AND Sr-ISOTOPE RATIOS

The following characterization of the Atana and Toconao ignimbrite compositions is based on unaltered pumice samples, with all analyses normalized to a 100% volatile-free basis. Only representative analyses are presented in Table 6. The full dataset shown in the figures is available as a supplementary datafile on the *Journal of Petrology* website at http://www.petrology.oupjournals.org. Toconao data represent pumices from the lower, unwelded and non-vapour-phase altered facies of the ignimbrite, and all Atana pumice samples represent the outflow facies because the intracaldera Atana ignimbrite is welded, devitrified and altered. Chemical evidence for alteration is lacking and the compositions reported are considered to represent the erupted magmas.

All Atana and Toconao pumices belong to the high-K suite of calc-alkaline magmas (Fig. 6), and are metaluminous to weakly peraluminous, with molar (Na + K)/Al between 0·6 and 0·9, and molar Al/(Ca + Na + K) between 1·0 and 1·3. Atana crystal-rich pumices are dacitic to rhyodacitic, with 66–70 wt % SiO_2, whereas the Toconao pumices and Atana crystal-poor pumices are high-silica rhyolites, with 76–77 wt % SiO_2 (Fig. 6). Two samples of Toconao plinian pumice have 78 wt % SiO_2. Grey pumice inclusions from the Atana ignimbrite range in composition from 59 to 64 wt % SiO_2. Clasts of scoria and banded pumice exist in the Toconao ignimbrite but are very rare and only one sample of each could be collected; thus their significance cannot be interpreted. The scoria has a dacitic composition (64 wt % SiO_2) and the banded pumice clast has a rhyodacitic composition (68 wt % SiO_2) (Fig. 6).

Major element oxide data of the Atana and Toconao pumice samples form distinct groups on silica variation diagrams (Fig. 7a) separated by compositional gaps, and these groups correspond to the Atana crystal-rich pumices, the grey pumice inclusions in Atana, and the Toconao pumices. The Toconao data show little or no systematic variation with silica because the samples are already at the high-silica end of magma differentiation. The other groups define regular and generally negative correlations of element oxides with silica excepting K_2O, which increases (see Fig. 6), and Na_2O, which shows no correlation (Fig. 7a). Both Na_2O and K_2O concentrations in the pumices are strongly variable at higher SiO_2 contents, whereas the total alkali sum (Na_2O + K_2O) remains relatively constant.

The Atana grey pumice inclusions as a group have the lowest silica contents and the Toconao pumices the highest. The Atana crystal-rich pumice group plots between these two extremes. In terms of all diagrams plotted in Fig. 7a the three main groups of samples are collinear. The less abundant pumice types tend to plot outside the main groups of samples and in some cases they bridge the compositional gaps between them. Thus the rare crystal-poor Atana pumices are rhyolitic and plot in the field of Toconao pumice whereas the brown–white banded Toconao pumice has a composition intermediate between

Table 2: Representative microprobe analyses of feldspar from Atana crystal-rich pumices and grey pumice inclusions and Toconao pumice

	Atana crystal-rich pumice								Atana grey pumice inclusions						Toconao pumice							
Sample:	Lari-96h-6		Lari-96h-5		Loy-97h-2		Loy-97h-2		Pujs-96h-10		Pujs-96h-10		Lari-96h-10		Toc-97h-3		Toc-97h-3		Quis-96h-21b		Quis-96h-21b	
Mineral:	plagioclase		plagioclase		plagioclase		sanidine		plagioclase		plagioclase		plagioclase		plagioclase		sanidine		plagioclase		sanidine	
	core	rim	core	rim	core	rim	core	rim	core	rim	core	rim	core	rim	core	rim	core	rim	core	rim	core	rim
SiO_2	51·6	56·4	55·9	58·6	61·0	60·3	65·1	65·2	57·8	58·7	52·2	58·3	57·9	56·5	63·6	64·2	66·3	64·9	64·0	64·0	65·6	65·6
Al_2O_3	31·0	28·2	27·1	25·1	25·0	25·6	19·1	19·1	26·3	26·0	29·2	26·0	26·5	27·5	22·6	22·4	18·9	19·1	22·6	22·4	18·9	18·8
FeO_t	0·3	0·3	0·3	0·3	0·2	0·3	0·1	0·1	0·2	0·3	0·5	0·3	0·3	0·3	0·1	0·0	0·1	0·1	0·1	0·1	0·1	0·0
CaO	14·0	10·3	10·0	7·7	6·8	7·3	0·2	0·3	8·8	8·1	12·2	8·0	8·8	10·1	4·0	3·7	0·2	0·2	3·9	3·8	0·2	0·2
Na_2O	3·6	5·5	5·4	6·5	7·2	6·9	2·7	2·6	6·4	6·8	4·6	6·6	6·3	5·8	8·2	8·4	3·9	3·6	8·7	8·9	3·6	3·7
K_2O	0·2	0·4	0·4	0·7	1·0	0·8	11·9	12·1	0·6	0·6	0·3	0·6	0·7	0·5	1·0	1·1	10·5	10·1	1·0	1·0	10·2	10·1
BaO	0·0	0·0	0·1	0·0	0·1	0·1	1·5	1·5	0·0	0·1	0·1	0·1	n.d.	n.d.	0·0	0·0	0·5	2·0	0·1	0·0	0·7	0·8
Total	100·6	101·0	99·2	98·9	101·3	101·3	100·6	100·9	100·1	100·5	98·9	100·0	100·6	100·6	99·7	99·8	100·3	100·0	100·2	100·2	99·1	99·2
Ab	31	48	48	58	62	60	25	25	55	58	40	58	54	49	74	75	36	35	76	76	35	36
Or	1	2	2	4	5	5	73	74	3	3	1	4	4	3	6	6	64	64	6	6	64	64
An	68	50	49	38	32	35	1	1	42	39	59	39	42	48	20	18	1	1	19	18	1	1
T (°C)																						
G						782										731				737		
F&L						756										731				744		
G&U						790										755				734		

Data represent spot analyses. Oxides in wt %; An, Ab, Or in mol %. n.d., not determined. Temperatures are derived from two-feldspar thermometry, and represent averages of T_{Or}, T_{Ab} and T_{An} calculated from rim analyses. Calibrations: G, Ghiorso (1984); F&L, Fuhrman & Lindsley (1988); G&U, Green & Usdansky (1986).

Table 3: Representative microprobe analyses of biotite from Atana crystal-rich pumices and grey pumice inclusions, and Toconao tuff and pumice

	Atana crystal-rich pumice				Atana grey pumice inclusion				Toconao tuff and pumice		
Sample:	Loy-97h-2		Lari-96h-6		Quis-96h-8		Pujs-96h-10		Toc-96h-4		Quis-96h-21b
	core	rim	core	rim	core	rim	core	rim	core	rim	core
SiO_2	37·5	37·0	37·3	36·9	36·9	36·9	37·8	37·3	37·3	37·4	37·5
TiO_2	4·6	4·8	4·8	4·7	4·9	4·8	4·8	4·9	4·3	4·3	3·4
Al_2O_3	14·4	13·7	13·6	13·4	13·8	13·6	13·6	13·3	13·6	13·8	14·0
Na_2O	0·4	0·4	0·4	0·4	0·5	0·5	0·3	0·4	0·5	0·6	0·5
K_2O	8·9	9·1	9·1	8·7	9·0	8·9	8·0	8·4	8·1	8·2	8·2
FeO_t	17·5	17·7	17·7	17·2	18·4	18·6	16·7	17·3	15·9	16·2	16·8
MnO	0·2	0·2	0·2	0·2	0·2	0·2	0·3	0·3	0·4	0·5	0·6
MgO	12·5	13·1	13·4	13·2	12·6	12·6	13·7	13·7	14·3	14·1	13·4
CaO	0·2	0·0	0·0	0·0	0·0	0·0	0·0	0·0	0·0	0·0	0·0
BaO	0·3	0·2	0·3	0·5	0·4	0·4	0·5	0·3	0·5	0·4	0·2
F	0·9	0·4	0·3	0·8	0·3	0·2	0·4	0·4	0·8	0·8	1·0
Cl	0·2	0·2	0·2	0·2	0·2	0·2	0·2	0·2	0·1	0·1	0·2
O=F	−0·38	−0·15	−0·11	−0·33	−0·11	−0·07	−0·16	−0·16	−0·32	−0·32	−0·42
O=Cl	−0·04	−0·04	−0·04	−0·04	−0·04	−0·04	−0·04	−0·04	−0·03	−0·03	−0·04
Total	97·0	96·4	97·1	95·7	96·9	96·8	96·0	96·4	95·4	96·0	95·2
mg-no.	0·56	0·57	0·57	0·58	0·55	0·55	0·59	0·59	0·62	0·61	0·59

Data represent spot analyses. Oxides in wt %. *mg*-number = molar Mg/(Mg + Fe_{total}).

the Atana crystal-rich pumice and Toconao pumice. The Toconao scoria sample has SiO_2 contents corresponding to the low-silica end of the Atana pumice range but it deviates from the latter in terms of MgO, Fe_2O_3 and MnO (latter two diagrams not shown in Fig. 7).

Trace element concentrations of Atana and Toconao pumices also cluster in variation diagrams (Fig. 7b) but, unlike the major elements, the trace element variations within and among the different groups do not define collinear trends. The rhyolitic samples, including Toconao pumice and Atana crystal-poor pumice, are generally depleted in Zr and Sr, and enriched in Rb, Nb and Y relative to the dacitic Atana crystal-rich pumice and grey pumice inclusions. They show a much greater range in Ba and Rb/Sr values than the dacitic pumices. The Atana crystal-poor pumices plot in or near the field of Toconao pumices and share the same compositional trends in Fig. 7b. Interestingly, some of the considerable variation in element abundances for the Toconao pumices correlates with geographical distribution of the outflow ignimbrite. Pumices from the east and southwest of the caldera tend to have higher K_2O, Rb, Nb and Y, lower Ba and Na_2O, and slightly lower Zr than those from the west of the caldera. It should be noted that the compositional range in Atana crystal-poor pumices is even greater than that of the Toconao pumices but the variation in the Atana samples does not correlate with location.

Chondrite-normalized REE patterns of Atana and Toconao pumices show that, although both magmas are light REE (LREE) enriched, the Atana samples have higher LREE/HREE (heavy REE) ratios (Fig. 8); the values of $(La/Yb)_N$ are 9–12 for Atana and 3–7 for Toconao. All samples are characterized by negative Eu anomalies and the magnitude of the anomaly increases regularly with increasing SiO_2: Eu/Eu* = 0·6–0·7 in the grey pumice inclusions, 0·6 in the Atana crystal-rich pumices and 0·5 in the Toconao pumices (Eu* is calculated as the geometric mean of normalized Sm and Gd). Toconao pumices have similar HREE abundances to the Atana crystal-rich pumices and have lower LREE and Eu abundances. The REE variations in the Toconao pumices also show a dependence on sample location. The Toconao pumices from east of the caldera have lower LREE and Eu than those from the west (Fig. 8).

Table 4: Representative microprobe analyses of amphibole from Atana crystal-rich pumices and grey pumice inclusions

	Atana crystal-rich pumice							Atana grey pumice inclusion		
Sample:	Loy-97h-5	Lari-96h-6	Loy-97h-2	Vent-97h-2	Jama-97h-1a	Jama-97h-2a	Lari-96h-5	Pujs-96h-10	Quis-96h-8	Lari-96h-5
SiO_2	44·9	46·1	45·9	46·0	46·0	46·0	45·2	47·6	45·4	46·5
TiO_2	1·8	1·7	1·7	1·6	1·7	1·5	1·7	1·4	1·6	1·5
Al_2O_3	8·5	8·3	8·1	7·8	8·1	7·5	8·4	7·0	8·7	8·0
Na_2O	1·5	1·4	1·4	1·5	1·5	1·4	1·6	1·3	1·5	1·5
K_2O	1·1	1·0	1·0	0·8	1·0	0·9	1·0	0·7	1·0	0·8
FeO_t	15·6	15·3	15·6	14·8	15·4	15·2	14·7	14·2	16·0	15·0
MnO	0·6	0·4	0·4	0·6	0·6	0·6	0·5	0·6	0·4	0·6
MgO	13·4	12·8	12·7	13·4	13·9	13·9	12·5	14·3	12·2	13·0
CaO	11·6	11·9	11·6	11·6	11·9	11·8	11·4	11·8	11·4	11·6
Total	99·0	98·8	98·5	98·0	100·0	98·7	96·8	98·8	98·2	98·5
mg-no.	0·65	0·60	0·60	0·64	0·66	0·67	0·59	0·66	0·57	0·61
% An	38	38	38	38	38	38	38	41	41	39
T (°C)	708	757	760	755	713	677	767	754	770	762
ΣAl	1·5	1·5	1·4	1·4	1·4	1·3	1·5	—	—	—
P (MPa)	235	224	213	192	199	163	236	—	—	—

Data represent spot analyses. Oxides in wt %. *mg*-number = molar Mg/(Mg + Fe^{2+}); ferric and ferrous Fe recalculated to determine *mg*-number using stoichiometric criteria after Droop (1987). Temperatures were calculated by hornblende–plagioclase thermometry (Holland & Blundy, 1994) using average plagioclase rim compositions with anorthite content % An. Pressure was determined by Al-in-hornblende barometry following the method of Anderson & Smith (1995), and pressures calculated for a temperature of 780°C are shown. Total Al cations (ΣAl) is calculated based on 23 oxygens.

Isotopic ratios in the Atana crystal-rich pumices, grey pumice inclusions and the Toconao pumices overlap. Initial $^{87}Sr/^{86}Sr$ ratios in Atana pumices range from 0·7094 to 0·7116, and the Toconao samples have values of 0·7106–0·7131. $^{143}Nd/^{144}Nd$ ranges from 0·512260 ($\varepsilon_{Nd} = -7·3$) to 0·512224 ($\varepsilon_{Nd} = -8·1$) in the Atana, and from 0·512256 ($\varepsilon_{Nd} = -7·4$) to 0·512217 ($\varepsilon_{Nd} = -8·2$) in the Toconao (Fig. 9, inset; Table 6). The spread in Sr isotopic ratios, in particular, is greater than would be consistent for a closed-system magma evolution. Correlations of isotope ratios with chemical variables such as SiO_2 were tested but not found. Ratios of $^{206}Pb/^{204}Pb$ and $^{208}Pb/^{204}Pb$ for all samples analysed fall within the narrow ranges 18·907–18·999 and 38·055–39·147, respectively. In terms of the Pb-isotopic domains outlined by Aitcheson *et al.* (1995), the La Pacana rocks have compositions that correspond to the Southern Altiplano domain, which agrees with the geographical location of La Pacana caldera with respect to the proposed domain boundaries.

GLASS COMPOSITION

Glass compositions from quartz-hosted melt inclusions in two Atana crystal-rich pumice samples and from matrix glass separates of one Toconao and two Atana pumices are presented in Table 7 and Fig. 10. The Atana pumice glasses, both from melt inclusions and matrix separates, plot well within the compositional field of the Toconao bulk pumice samples and resemble the crystal-poor Atana pumices. This implies that the compositional differences between the Atana crystal-rich pumice and Toconao pumices are primarily a function of different crystal contents. The fractionation vectors shown in Fig. 10 show that the separate compositional groups defined by Atana crystal-rich pumice and Toconao pumice can be related by simple fractionation of observed phases in the Atana samples. Also evident from Fig. 10 is that the Toconao glass is similar to the bulk pumice, as expected from the low crystal contents in the pumice, but the glass is slightly more fractionated (i.e. lower Zr, Sr and Ba contents) and has more variable Rb concentrations.

Table 5: Representative microprobe analyses of magnetite and ilmenite from the Toconao pumice, Atana crystal-rich pumice and grey pumice inclusions

	Toconao pumice		Atana crystal-rich pumice										Atana grey pumice inclusion					
Sample:	Quis-96h-4a		Loy-97h-5		Jama-97h-2a		Quis-96h-9		Jama-97h-3		Vent-97h-2		Pujs-96h-10		Lari-96h-10		Lari-97h-5	
Mineral:	mag	ilm	mag	ilm	mag	ilm	mag	ilm	mag	ilm	mag	ilm	mag	ilm	mag	ilm	mag	ilm
SiO_2	0·1	0·0	0·1	0·2	0·3	0·0	0·1	0·0	n.d.	0·0	n.d.	0·0	n.d.	0·1	0·1	0·0	0·1	0·0
TiO_2	4·0	39·6	6·1	44·1	5·9	41·2	4·9	35·6	5·4	38·4	5·3	40·5	4·9	40·1	4·7	39·4	5·7	39·9
Al_2O_3	1·5	0·1	1·3	0·0	1·4	0·1	1·4	0·1	1·4	0·0	1·8	0·1	1·7	0·0	1·4	0·1	1·2	0·0
FeO_t	85·3	52·7	83·6	52·2	85·7	54·9	85·4	57·5	84·4	54·8	84·1	52·3	86·3	52·8	87·2	55·2	87·4	56·4
FeO	32·8	31·9	34·6	35·4	35·2	33·1	33·8	28·9	33·8	30·8	33·7	31·9	33·9	31·8	34·0	31·9	35·0	32·0
Fe_2O_3	58·4	23·2	54·5	18·7	56·3	24·2	57·5	31·8	56·3	26·8	56·1	22·7	58·4	23·3	59·2	26·0	58·3	27·2
MnO	0·9	1·7	0·6	1·2	1·0	1·4	0·7	1·0	0·9	1·3	0·7	1·4	0·8	1·5	0·8	1·2	1·0	1·4
MgO	0·5	1·0	0·7	1·8	0·8	1·4	0·7	1·2	0·7	1·3	0·8	1·7	0·8	1·6	0·7	1·3	0·8	1·4
Total	98·1	97·5	97·9	101·4	100·9	101·4	99·0	98·6	98·5	98·6	98·5	98·4	100·5	98·4	100·8	99·9	102·0	101·9
Log (Mg/Mn)	−0·02	0·03	0·31	0·43	0·12	0·25	0·26	0·31	0·13	0·25	0·32	0·32	0·28	0·28	0·21	0·28	0·10	0·22
T (°C)		744		774		785		796		790		776		765		765		789
Log fO_2		−12·8		−12·9		−12·3		−11·7		−12·0		−12·5		−12·6		−12·4		−12·1

Data represent spot analyses. Oxides in wt %. Ferric and ferrous Fe recalculated on stoichiometric criteria after Droop (1987). Temperatures and oxygen fugacities determined by Fe–Ti oxide thermometry using the QUILF program of Andersen *et al.* (1993). Log Mg/Mn (atomic) ratios of equilibrium magnetite–ilmenite pairs calculated after Bacon & Hirschmann (1988).

Table 6: Representative chemical and isotopic compositions of Atana and Toconao pumices

	Atana pumices							
Sample:	Lari-96h-6 x-rich	Quis-96h-9 x-rich	Lari-96h-8 x-rich	Lari-96h-10 grey	Pujs-96h-10 grey	Lari-96h-9 grey	Vent-97h-4a x-poor	Pujs-96h-13a x-poor
SiO_2	68·0	66·1	67·8	58·6	60·2	58·3	72·3	73·8
TiO_2	0·51	0·59	0·54	0·95	1·12	1·18	0·19	0·09
Al_2O_3	15·0	15·6	14·8	16·4	16·4	16·9	13·4	12·6
Fe_2O_{3t}	3·06	3·69	3·28	6·32	6·35	6·62	1·20	0·57
MnO	0·06	0·07	0·06	0·14	0·14	0·14	0·05	0·06
MgO	1·08	1·30	1·17	2·82	2·37	2·64	0·30	0·10
CaO	3·02	3·36	3·01	5·57	5·25	5·75	1·13	0·66
Na_2O	2·91	3·28	2·99	3·29	3·35	3·39	1·88	3·54
K_2O	4·10	3·57	4·30	3·40	3·08	3·03	4·38	4·97
P_2O_5	0·13	0·15	0·13	0·22	0·20	0·28	0·07	0·03
H_2O	1·50	1·77	1·79	1·57	1·27	1·39	4·07	2·54
CO_2	0·12	0·13	0·03	0·06	0·07	0·09	0·09	0·08
Total	99·46	99·66	99·89	99·36	99·75	99·67	99·04	99·04
Ba	585	647	599	457	532	386	839	270
Cr	13	<10	<10	16	11	10	<10	<10
Rb	195	161	216	151	136	126	189	281
Sr	247	262	228	279	302	295	186	47
V	64	81	65	152	187	168	19	<10
Y	26	25	23	21	30	24	15	22
Zn	53	72	49	85	96	84	32	27
Zr	171	189	172	182	184	211	87	52
Nb	14	16	14	11	17	15	11	18
Th	22	21	n.d.	15	17	n.d.	n.d.	n.d.
U	7·1	6·4	n.d.	4·7	5·5	n.d.	n.d.	n.d.
Pb	11	21	n.d.	15	16	n.d.	n.d.	n.d.
Li	18	43	n.d.	24	29	n.d.	n.d.	n.d.
Cs	15	17	n.d.	9	11	n.d.	n.d.	n.d.
Ta	1·6	1·6	n.d.	1·0	1·4	n.d.	n.d.	n.d.
La	43	40	n.d.	36	38	n.d.	n.d.	n.d.
Ce	82	78	n.d.	72	78	n.d.	n.d.	n.d.
Pr	10	10	n.d.	9	10	n.d.	n.d.	n.d.
Nd	34	33	n.d.	32	36	n.d.	n.d.	n.d.
Sm	6·5	6·5	n.d.	6·3	7·4	n.d.	n.d.	n.d.
Eu	1·1	1·2	n.d.	1·2	1·5	n.d.	n.d.	n.d.
Gd	5·3	5·4	n.d.	5·4	6·5	n.d.	n.d.	n.d.
Tb	0·84	0·82	n.d.	0·86	1·10	n.d.	n.d.	n.d.
Dy	4·6	4·8	n.d.	4·6	5·7	n.d.	n.d.	n.d.
Ho	0·83	0·85	n.d.	0·88	1·10	n.d.	n.d.	n.d.
Er	2·5	2·5	n.d.	2·5	3·0	n.d.	n.d.	n.d.
Tm	0·36	0·37	n.d.	0·37	0·48	n.d.	n.d.	n.d.
Yb	2·4	2·5	n.d.	2·4	2·9	n.d.	n.d.	n.d.
Lu	0·38	0·39	n.d.	0·40	0·48	n.d.	n.d.	n.d.
Sc	7·8	9	n.d.	16	18	n.d.	n.d.	n.d.
$^{87}Sr/^{86}Sr$	0·710428	0·711712	n.d.	0·709469	0·709981	n.d.	n.d.	n.d.
$^{87}Sr/^{86}Sr_i$	0·710293	0·711607	n.d.	0·709377	0·709904	n.d.	n.d.	n.d.
$^{143}Nd/^{144}Nd$	0·512234	0·512224	n.d.	0·512260	0·512229	n.d.	n.d.	n.d.
$\varepsilon Nd_{(T)}$	−7·83	−8·07	n.d.	−7·33	−7·94	n.d.	n.d.	n.d.
$^{206}Pb/^{204}Pb$	18·998	18·999	n.d.	18·976	n.d.	n.d.	n.d.	n.d.
$^{208}Pb/^{204}Pb$	39·103	39·107	n.d.	39·051	n.d.	n.d.	n.d.	n.d.
$^{207}Pb/^{204}Pb$	15·691	15·693	n.d.	15·679	n.d.	n.d.	n.d.	n.d.

	Toconao pumices							
Sample:	Jama-96h-7b tube	Toc-97h-2 tube	Toc-96h-2a tube	Quis-96h-21a x-poor	Quis-96h-4b x-poor	Quis-96h-20a x-poor	Toc-97h-1A plinian	Toc-C 97h-1 plinian
SiO_2	73·4	73·7	74·1	74·1	74·2	73·9	74·6	74·0
TiO_2	0·10	0·12	0·12	0·10	0·10	0·13	0·11	0·11
Al_2O_3	12·6	12·5	12·5	12·8	12·7	12·9	11·8	12·1
Fe_2O_{3t}	0·61	0·69	0·64	0·63	0·52	0·79	0·65	0·67
MnO	0·07	0·07	0·07	0·07	0·07	0·07	0·06	0·06
MgO	0·08	0·08	0·09	0·08	0·10	0·15	0·08	0·09
CaO	0·61	0·55	0·56	0·54	0·61	0·60	0·52	0·67
Na_2O	3·36	3·59	3·57	2·82	2·75	3·54	3·27	3·40
K_2O	5·06	4·69	4·70	5·70	5·04	4·77	4·53	4·45
P_2O_5	0·03	0·02	0·02	0·03	0·03	0·04	0·02	0·03
H_2O	3·15	3·26	2·70	2·26	3·05	2·45	3·91	3·76
CO_2	0·05	0·08	0·07	0·09	0·09	0·08	0·07	0·07
Total	99·14	99·33	99·17	99·24	99·27	99·45	99·56	99·41
Ba	532	603	700	536	444	446	622	628
Cr	11	<10	<10	<10	<10	<10	<10	<10
Rb	223	219	214	257	242	218	215	211
Sr	37	47	49	43	37	48	44	63
V	<10	<10	<10	<10	<10	<10	<10	<10
Y	28	28	26	28	29	30	24	25
Zn	45	40	43	35	30	47	39	40
Zr	67	75	75	66	63	70	68	68
Nb	20	19	20	19	21	22	20	19
Th	16	n.d.	n.d.	16	16	n.d.	n.d.	n.d.
U	8·1	n.d.	n.d.	8·4	9·1	n.d.	n.d.	n.d.
Pb	20	n.d.	n.d.	17	16	n.d.	n.d.	n.d.
Li	70	n.d.	n.d.	29	29	n.d.	n.d.	n.d.
Cs	25	n.d.	n.d.	23	28	n.d.	n.d.	n.d.
Ta	1·9	n.d.	n.d.	2·0	2·1	n.d.	n.d.	n.d.
La	14	n.d.	n.d.	15	13	n.d.	n.d.	n.d.
Ce	35	n.d.	n.d.	31	26	n.d.	n.d.	n.d.
Pr	5	n.d.	n.d.	4	4	n.d.	n.d.	n.d.
Nd	16	n.d.	n.d.	16	14	n.d.	n.d.	n.d.
Sm	4·4	n.d.	n.d.	4·3	3·9	n.d.	n.d.	n.d.
Eu	0·7	n.d.	n.d.	0·7	0·6	n.d.	n.d.	n.d.
Gd	4·4	n.d.	n.d.	4·3	4·1	n.d.	n.d.	n.d.
Tb	0·82	n.d.	n.d.	0·74	0·81	n.d.	n.d.	n.d.
Dy	4·9	n.d.	n.d.	4·8	4·9	n.d.	n.d.	n.d.
Ho	0·93	n.d.	n.d.	0·93	0·94	n.d.	n.d.	n.d.
Er	2·8	n.d.	n.d.	2·7	2·8	n.d.	n.d.	n.d.
Tm	0·45	n.d.	n.d.	0·40	0·40	n.d.	n.d.	n.d.
Yb	2·7	n.d.	n.d.	2·7	2·7	n.d.	n.d.	n.d.
Lu	0·42	n.d.	n.d.	0·42	0·41	n.d.	n.d.	n.d.
Sc	4·5	n.d.	n.d.	4·4	4·4	n.d.	n.d.	n.d.
$^{87}Sr/^{86}Sr$	0·711687	n.d.	n.d.	0·712941	0·714324	n.d.	n.d.	n.d.
$^{87}Sr/^{86}Sr_i$	0·710560	n.d.	n.d.	0·711823	0·713055	n.d.	n.d.	n.d.
$^{143}Nd/^{144}Nd$	0·512252	n.d.	n.d.	0·512217	0·512256	n.d.	n.d.	n.d.
$\varepsilon Nd_{(T)}$	−7·51	n.d.	n.d.	−8·19	−7·44	n.d.	n.d.	n.d.
$^{206}Pb/^{204}Pb$	18·992	n.d.	n.d.	18·995	n.d.	n.d.	n.d.	n.d.
$^{208}Pb/^{204}Pb$	39·133	n.d.	n.d.	39·147	n.d.	n.d.	n.d.	n.d.
$^{207}Pb/^{204}Pb$	15·673	n.d.	n.d.	15·678	n.d.	n.d.	n.d.	n.d.

n.d., not determined. Total Fe expressed as Fe_2O_3.

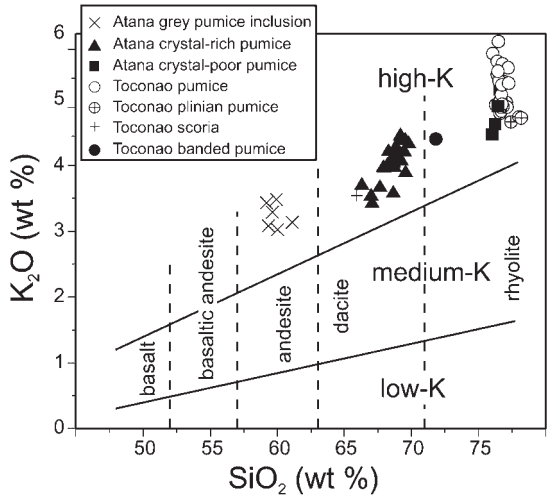

Fig. 6. K_2O vs SiO_2 classification diagram for Atana and Toconao pumices. Fields from Le Maitre (1989).

ESTIMATION OF INTENSIVE PARAMETERS, VISCOSITY AND DENSITY

Mineral equilibrium temperatures and pressures, H_2O, viscosity and density were determined for Atana and Toconao pumices to gain insights into the pre-eruptive conditions in the La Pacana magma chamber. Mineral rim compositions were used in all calculations, as these were considered most likely to reflect the last magmatic equilibrium conditions. Where possible, tests for homogeneity and equilibrium were applied [e.g. for Fe–Ti oxides following the method of Bacon & Hirschmann (1988)].

Temperature and fO_2

Four independent geothermometers were applied: magnetite–ilmenite, two-feldspar, hornblende–plagioclase

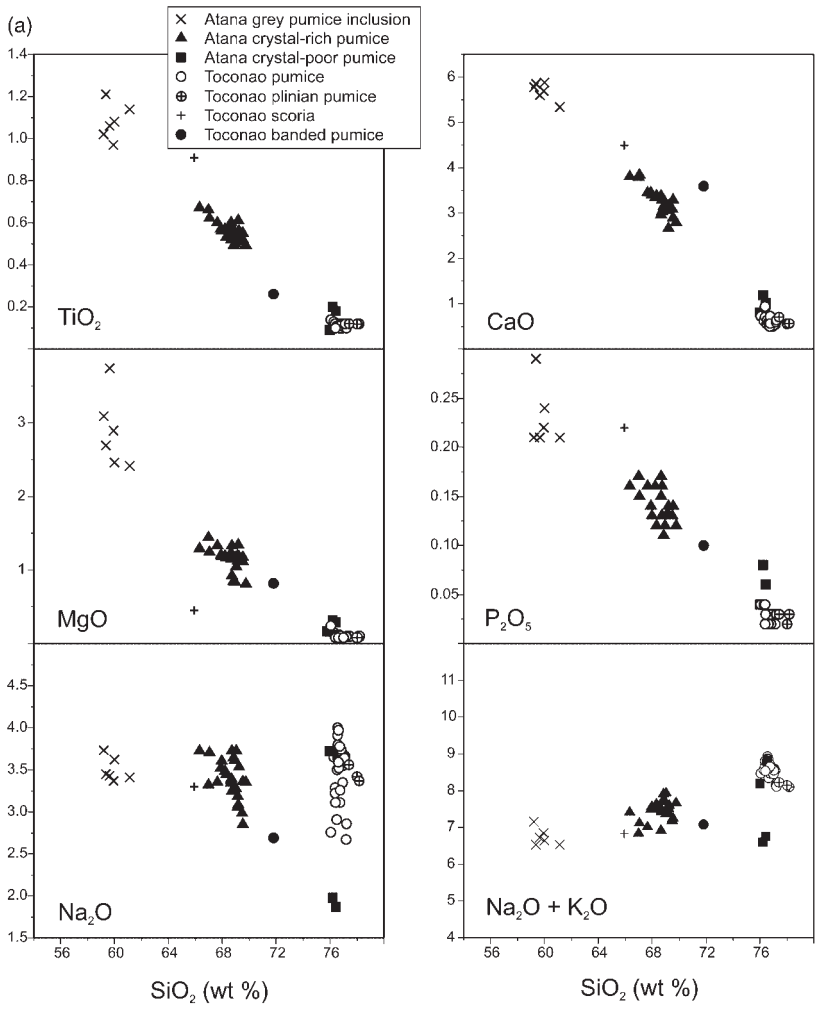

Fig. 7. (a).

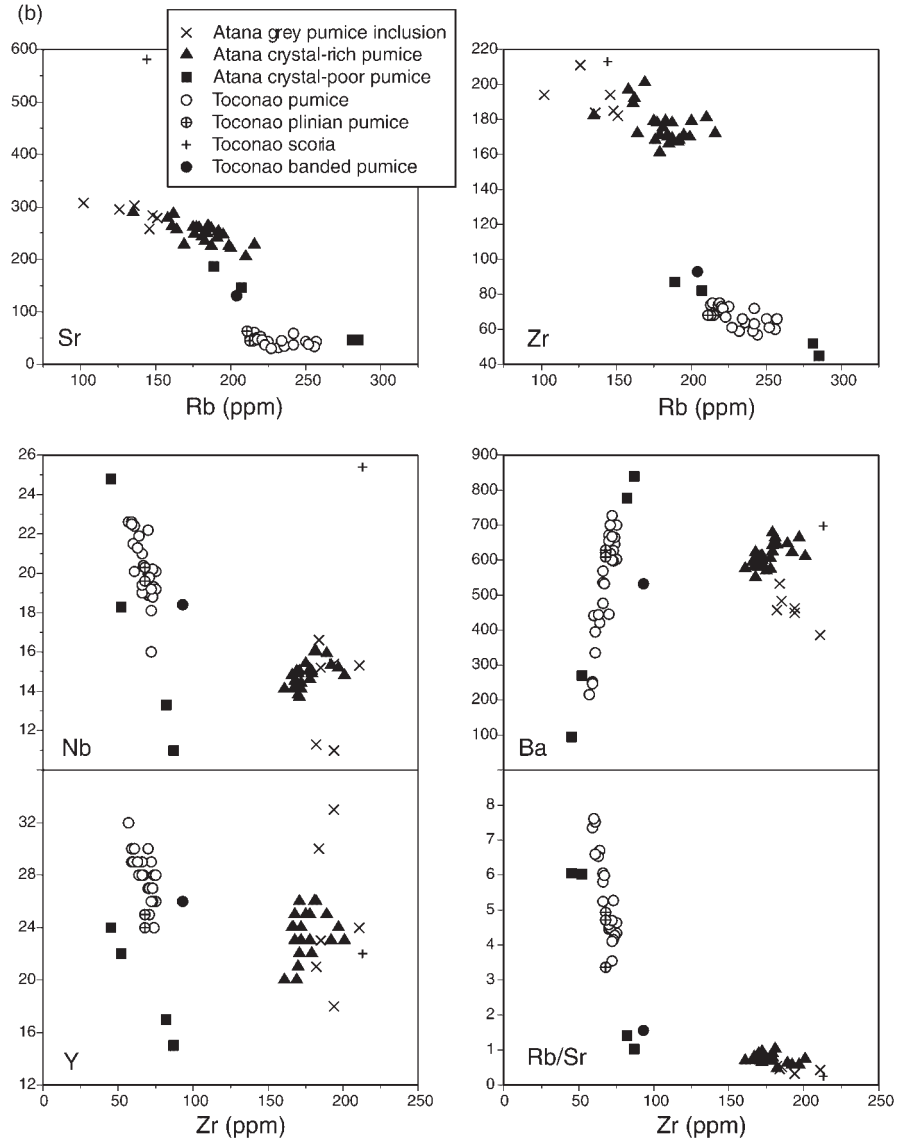

Fig. 7. (a) Major element and (b) trace element variation diagrams of Atana and Toconao pumices. Analyses in (a) are normalized on a 100% anhydrous basis.

and zircon saturation thermometry using the calibrations described below (Tables 2, 4 and 5 and Fig. 11). The two-oxide geothermometer is independent of pressure. Pressure-dependent two-feldspar and hornblende–plagioclase thermometery was carried out for pressures derived from Al-in-hornblende barometry.

Two-oxide thermometry calculations were carried out on 22 mineral pairs from nine samples using the solution model of Andersen & Lindsley (1988) following the method of Andersen *et al.* (1993). In Fig. 11 the average mineral-pair temperature from each sample is plotted, and the error bar reflects the largest 2σ deviation from the mean in the sample suite. For the Atana crystal-rich pumices, the average temperatures range from 770 to 790°C (Table 5). A similar temperature range of 725–790°C was obtained for the grey pumice inclusions using this method. A single Toconao sample with co-existing magnetite and ilmenite yielded an average temperature of 740°C. Log fO_2 values range from $-11{\cdot}5$ to $-13{\cdot}5$ for the Atana and Toconao ignimbrites. These values lie three log units above the quartz–fayalite–magnetite buffer at the temperatures indicated, and overlap with the field defined by the Fish Canyon Tuff (Whitney & Stormer, 1985).

Two-feldspar temperatures were calculated for eight mineral pairs in five samples using the calibrations of

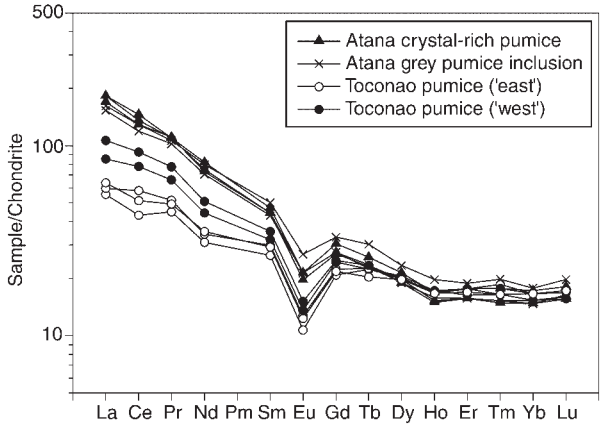

Fig. 8. Chondrite-normalized REE patterns for the Atana and Toconao. Normalizing values from Anders & Grevesse (1989).

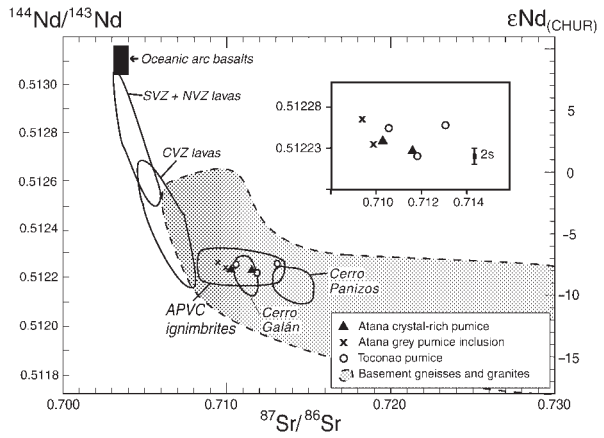

Fig. 9. Initial $^{144}Nd/^{143}Nd$ and $^{87}Sr/^{86}Sr$ ratios for Atana and Toconao pumices compared with the range for Pliocene–Quaternary andesitic–dacitic effusive rocks in the Andes and Proterozoic–Mesozoic basement rocks in Northern Chile and NW Argentina (present-day compositions; Lucassen *et al.*, 1999). The La Pacana samples fall within the field representing large-volume, crystal-rich APVC ignimbrites, and overlap the Cerro Galán field [data from Francis *et al.* (1989)]. The field for the Panizos ignimbrites (Ort *et al.*, 1996) is plotted separately for clarity, as this centre has slightly more radiogenic Sr ratios than the other APVC centres. Enlarged region shows La Pacana data. APVC field based on data from Lindsay (1999) and Schmitt (1999); Southern and Northern Volcanic Zone (SVZ and NVZ) field based on data from Futa & Stern (1988), Hildreth & Moorbath (1988), Rogers & Hawkesworth (1989), López-Escobar *et al.* (1991) and Tormey *et al.* (1991); Central Volcanic Zone (CVZ) lavas field based on data from James (1982), Rogers & Hawkesworth (1989) and Trumbull *et al.* (1999); oceanic arc basalt field from Zartman & Haines (1988).

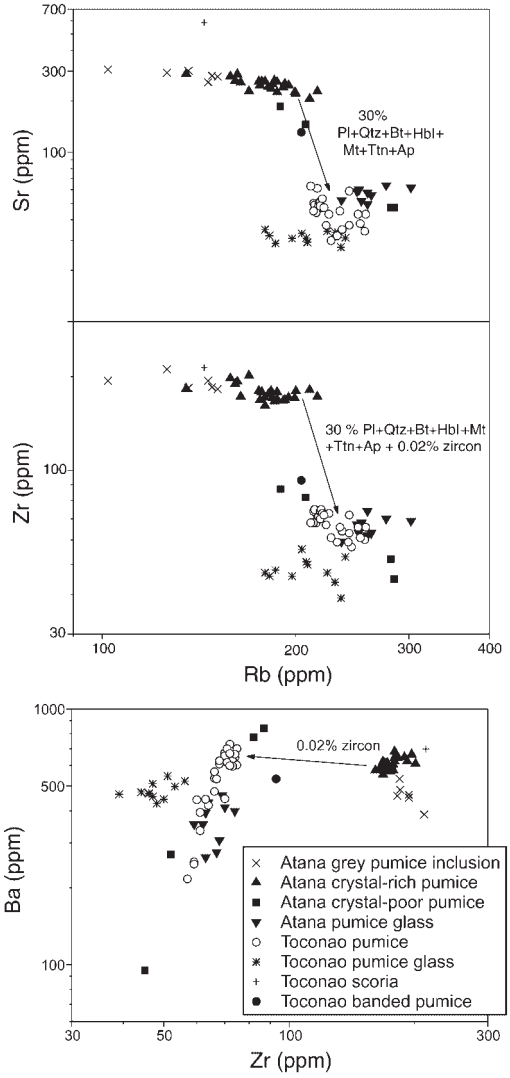

Fig. 10. Variation diagrams comparing Atana and Toconao glass compositions (determined by SIMS analyses) with pumice populations. Also shown are vectors representing fractionation paths (see text). (See Table 1 for mineral abbreviations.)

Ghiorso (1984), Green & Usdansky (1986) and Fuhrman & Lindsley (1988), which take into consideration effects of Al–Si ordering. Differences in T_{Or}, T_{Ab} and T_{An} were minimized by adjusting the two given feldspar compositions within a 2 mol % uncertainty, based on the algorithm developed by Fuhrman & Lindsley (1988) to account for typical analytical imprecision. There is generally good agreement among the three calibrations for the feldspar thermometers for the Toconao pumices, all yielding temperatures between 710 and 755°C. The agreement is not as good for the Atana feldspar pairs, with the Fuhrman & Lindsley (1988) calibration yielding lower temperatures than the other calibrations. Hence, the range of two-feldspar temperatures for the Atana is considerable (705–790°C). The reason for this is not clear. Temperatures obtained from one feldspar pair from an Atana crystal-poor pumice average 710°C, which lies at the lower end of the Toconao two-feldspar temperature range. The error for all three two-feldspar thermometers used is considered to be ± 50°C (Kroll *et al.*, 1993).

Table 7: Chemical composition of melt inclusions in quartz and matrix glass from two Atana pumices, and matrix glass analyses from one Toconao pumice

Sample:	Lari-96h-5	Lari-96h-5	Lari-96h-5	Lari-96h-5	Lari-96h-5	Lari-96h-8	Lari-96h-8	Lari-96h-8	Lari-96h-8	Lari-96h-8	Toc-96h-2
Unit:	Atana	Atana	Atana	Atana	Atana	Atana	Atana	Atana	Atana	Atana	Toconao
Analysis:	MI1	MI2	MI3	MI4	matrix glass[a]	MI1	MI2	MI3	MI4	matrix glass[b]	matrix glass[c]
SiO_2	73·3	70·9	73·4	72·4	74·5	73·4	72·3	71·6	68·7	74·4	74·5
TiO_2	0·08	0·11	0·06	0·15	0·12	0·13	0·06	0·08	0·10	0·12	0·10
Al_2O_3	11·5	12·7	11·8	12·3	12·2	13·9	11·2	11·6	13·7	12·5	12·3
Fe_2O_{3t}	0·68	0·60	0·59	0·46	0·19	0·58	0·80	0·54	0·58	0·46	0·55
MnO	0·03	0·07	0·02	0·01	0·03	0·01	0·04	0·07	0·01	0·04	0·06
MgO	0·02	0·06	0·03	0·02	0·03	0·10	0·05	0·02	0·06	0·05	0·07
CaO	0·56	0·68	0·50	0·55	0·60	0·82	0·58	0·55	0·64	0·87	0·45
K_2O	4·86	5·16	4·96	5·15	5·61	5·49	4·61	4·81	5·35	5·44	4·69
Na_2O	3·59	3·56	3·54	3·81	2·54	3·50	3·41	3·77	4·49	2·77	3·22
P_2O_5	0·03	b.d.	0·05	b.d.	0·02	b.d.	b.d.	0·01	0·01	0·01	0·02
Total[d]	94·7	93·8	94·9	94·9	95·9	97·9	93·1	93·0	93·7	96·6	96·0
Total[e]	99·4	100·2	99·1	99·5		99·6	101·0	99·4	99·8		
Li	693	641	371	251	n.d.	n.d.	557	n.d.	423	n.d.	n.d.
B	43	58	43	42	n.d.	n.d.	47	n.d.	25	n.d.	n.d.
F	281	355	202	114	n.d.	n.d.	493	n.d.	314	n.d.	n.d.
Rb	239	277	233	234	264	n.d.	273	n.d.	164	251	221
Sr	44	40	21	17	57	n.d.	28	n.d.	48	57	31
Y	6	15	12	18	12	n.d.	16	n.d.	9	12	22
Zr	55	65	25	33	66	n.d.	62	n.d.	43	66	49
Nb	11	10	17	12	10	n.d.	14	n.d.	6	12	15
Ba	139	187	80	68	400	n.d.	115	n.d.	278	281	493
La	14	21	6	13	30	n.d.	19	n.d.	19	29	12
Ce	23	32	10	25	n.d.	n.d.	33	n.d.	35	n.d.	n.d.
Eu	0·4	1·1	0·1	0·4	n.d.	n.d.	0·3	n.d.	1·1	n.d.	n.d.
Th	17	29	6	16	26	n.d.	18	n.d.	24	26	11
U	8	11	6	8	n.d.	n.d.	10	n.d.	6	n.d.	n.d.
Cl	0·14	0·16	0·17	0·17	n.d.	0·17	0·13	0·16	0·23	n.d.	n.d.
H_2O	3·9	4·0	3·4	3·1	n.d.	n.d.	4·4	n.d.	3·6	n.d.	n.d.

[a]Majors, $n = 9$; traces, $n = 7$. [b]Majors, $n = 9$; traces, $n = 3$. [c]Majors, $n = 9$; traces, $n = 7$. [d]Sum of major elements with oxygen calculated stoichiometrically. [e]Original analytical total with oxygen analysed.
Major elements (oxides in wt %) were determined by electron microprobe. Trace elements (in ppm) and water contents (wt %) determined by SIMS. n.d., not determined; b.d., below detection limit. Matrix glass major element data represent the mean of nine glass shard analyses; trace element data the mean of between three and seven shard analyses.

The amphibole–plagioclase thermometer (Holland & Blundy, 1994) could be applied only to the Atana pumices (Fig. 11; Table 4). The range of average temperatures determined in each of four grey pumice inclusions is 723–770°C (mean 750°C). The corresponding range of average values from eight samples of Atana crystal-rich pumice is greater (675–800°C) but the mean temperature for all eight samples is similar to that of the grey inclusions, at 740°C. The uncertainty in the thermometer is considered to be ± 40°C (Holland & Blundy, 1994). These mean values are lower than the two-oxide temperatures, but near the median of the temperature range obtained by two-feldspar thermometry.

Zircon saturation thermometry based on Watson & Harrison (1983) yields ranges of 773–789°C for the Atana crystal-rich pumices, 749–763°C for the Atana grey

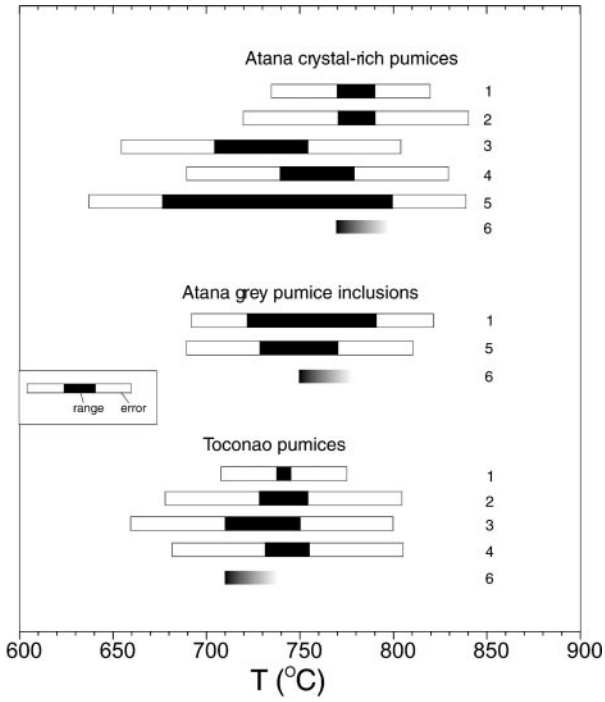

Fig. 11. Results of various thermometers and their errors. 1, Two-oxide (Andersen *et al.*, 1993); 2, two-feldspar (Green & Usdansky, 1986); 3, two-feldspar (Fuhrman & Lindsley, 1988); 4, two-feldspar (Ghiorso, 1984); 5, hornblende–plagioclase (Holland & Blundy, 1994); 6, Zr saturation (Watson & Harrison, 1983).

inclusions and 710–730°C for the Toconao pumices (Fig. 11). Zircons are present in all samples and therefore the magmas were saturated in Zr and the calculated temperatures represent minimum estimates.

In summary, and taking into consideration the minimum temperatures from zircon-saturation thermometry, our preferred temperature estimates for the crystallization conditions of the ignimbrite magmas are as follows: 770–790°C for the Atana pumice; 750–790°C for the Atana grey pumice inclusions and 730–750°C for the Toconao pumice (Fig. 11).

Pressure

The only suitable mineral barometer for these ignimbrites is Al-in-hornblende (e.g. Hammarstrom & Zen, 1986; Johnson & Rutherford, 1989; Anderson & Smith, 1995). The necessary mineral assemblage (plagioclase + biotite + hornblende + alkali feldspar + quartz + titanite + iron–titanium oxide) is present only in the Atana crystal-rich pumice samples. We applied the revised expression of Anderson & Smith (1995) because it takes into account the effects of temperature. A total of 24 amphibole rim compositions from eight samples were used, and calculations were carried out for three temperatures spanning the range obtained by two-oxide thermometry (this method provided the tightest temperature range for the Atana crystal-rich pumices; Table 4). Calculations using all hornblende analyses ($n = 24$) for the temperature range 770–790°C yield a total pressure range of 110–330 MPa. The average hornblende composition yields 190 and 230 MPa at 770 and 790°C, respectively, which corresponds to 7–8·5 km depth (assuming magma chamber pressure = lithostatic pressure, and a crustal density of 2·7). The total uncertainty in these values (σ_T) is high, $\sim$100 MPa, based on the error propagation equation $\sigma_T^2 = (\sigma_1^2 + \sigma_2^2 + \sigma_3^2)$, where σ_1 is the inherent uncertainty in calibration (50–60 MPa, Johnson & Rutherford, 1989; Anderson & Smith, 1995), σ_2 is 85 MPa from the propagated effect of a temperature error of 50°C; and σ_3 is 10 MPa, reflecting a 1% analytical error in Al (Anderson & Smith, 1995). Our average pressure estimates agree with estimated equilibration pressures of 200–300 MPa for the Fish Canyon Tuff using an earlier calibration of the same method (Johnson & Rutherford, 1989). They also agree with other estimates for young caldera complexes such as the Long Valley and Yellowstone calderas, where geological and geophysical evidence indicates pressures of 200–300 MPa for the tops of the present magma chambers (Smith & Braile, 1983; Christiansen, 1984; Sanders, 1984).

Volatile contents

Direct determination of H_2O by SIMS analysis in eight melt inclusions in quartz from two Atana pumice samples yielded 3·1–4·4 wt % (average 3·7 wt %) (Table 7). H_2O contents of the Atana magma were also estimated by the plagioclase–melt hygrometer of Housh & Luhr (1991) using the *P–T* estimates discussed above. Two independent calibrations are available, based on the equilibrium constants of exchange reactions for albite and anorthite components between plagioclase and melt. H_2O contents were calculated by this method using the program TWATER1 (provided by the authors), at a pressure of 200 MPa, and allowing temperatures to vary within the range determined from mineral thermometry (e.g. from 770 to 790°C for the Atana crystal-rich pumices). Atana pumice glass and plagioclase rim compositions from eight samples yield average H_2O contents of 4·5 $\pm$ 0·5 and 3·3 $\pm$ 0·3 wt % from the Ab and An models respectively, whereby the least difference between H_2O contents calculated by the Ab and An methods was observed at a temperature of 785°C, and plagioclase rim composition of $An_{30–36}$. Despite the differences between Ab and An model calibration results, these span the same range as those directly measured by SIMS.

In the absence of melt inclusion data from the crystal-poor Toconao ignimbrite, estimates of pre-eruptive H_2O

contents were obtained solely from the Housh & Luhr (1991) hygrometer. For temperatures of 730–750°C and a pressure of 200 MPa, calculated H_2O contents for the Toconao ignimbrite showed excellent agreement between the Ab and An solution models, yielding average values of 6·3 wt % and 6·8 wt %, respectively. The smallest difference between these two models was observed at a temperature of 730°C and plagioclase rim composition of $An_{18–21}$.

The water contents discussed above refer to the melt fraction only. In the case of Atana pumices, the H_2O content of ~3–4 wt % represents that of a residual melt following ~40% crystallization. Taking the modal proportion of anhydrous and hydrous crystals into account, the H_2O content of the total pre-eruptive magma would be ~2–3 wt %. As the Toconao magma was relatively crystal poor (~1% crystals), there is no significant difference between the H_2O contents in melt and bulk magma.

Viscosity and density

Reliable estimates of magma viscosity and density are important in constraining possible differentiation mechanisms and evaluating magma properties and possible eruption mechanisms. Magma viscosities were calculated from the *T*, H_2O and bulk composition data based on the method of Pinkerton & Stevenson (1992) and the results are $10^{6·0}$ Pa s for the Toconao magma (at 740°C, 1% crystals and 6% H_2O) and $10^{7·4}$–$10^{8·6}$ Pa s for the Atana (at 780°C, 40% crystals, and 4·4–3·1% H_2O). Densities were calculated according to the method of Lange (1994), using physical constants for minerals given by Ahrens (1995) and taking into consideration the modal proportion of crystals in the rock, volatile content, and glass/crystal ratios. Values of 2·25 kg/m^3 (at 740°C, 6% H_2O) were obtained for the pre-eruptive Toconao magma, and 2·49–2·51 kg/m^3 for that of the Atana (at 780°C, 4·4–3·1% H_2O). Water and crystal-free melt densities are the same for both units (2·39 kg/m^3).

DISCUSSION

Magma chamber conditions and differentiation processes

The Toconao and Atana ignimbrites have similar lateral distributions, they both thicken towards La Pacana caldera (Lindsay *et al.*, 2001), and the Toconao ignimbrite is directly overlain by the Atana ignimbrite at almost all localities (Fig. 2). These characteristics are consistent with both units coming from La Pacana caldera, and suggest that they may be cogenetic. Overlapping isotopic ratios for Atana and Toconao pumices support this idea.

Major element concentrations in the Atana and Toconao pumice samples define systematic trends that suggest the operation of fractionation in the Atana magma, with the Toconao pumices representing the residual magma and the grey pumice inclusions the extracted assemblage (Fig. 7a). The overall mineral assemblage and mineral rim compositions in the grey pumice inclusions are similar to those in the Atana pumice. Furthermore, there are no crenulate margins or reaction rims between the grey pumice inclusions and their host pumice as would be expected for xenoliths incorporated in a magma. The grey pumice inclusions are therefore considered to be cognate, and are interpreted as side-wall accumulations of early crystallized fractions of the Atana magma. The presence of less differentiated cores in some of the crystals in the inclusions is consistent with this, as is the lack of quartz and sanidine, both of which can be expected to form during the later stages of fractionation. The high crystal contents and fine grain size of these inclusions are interpreted as the result of a high thermal gradient at the chamber wall. Similar fine-grained, crystal-rich inclusions have also been recognized in many of the other APVC ignimbrites by de Silva (1989*c*), who discussed the interpretion of their origin as side-wall cumulates in more detail.

At first glance, however, the variations in trace elements do not support simple fractionation as suggested by the major elements (Fig. 7b), and there is a considerable compositional gap between the Atana and Toconao pumice fields. However, the similarity between the crystal-poor pumices from the lower portions of the Atana ignimbrite and pumices of the Toconao ignimbrite indicates that the basal unit in the Atana may represent a magma of the same composition as that of the Toconao. Furthermore, glass analyses from Atana crystal-rich pumices are very similar in composition to the Toconao tube pumices (Fig. 10), showing unequivocally that variation in major and trace element pumice chemistry can be explained by different crystal contents. Despite the lack of intermediate compositions, therefore, there is strong evidence that crystal fractionation is the process responsible for the compositional variability observed in the La Pacana suite.

Fractional crystallization model

Table 8 shows the results of least-squares modelling to test the possibility that the Atana and Toconao magmas are related by fractional crystallization. The model uses the most evolved Atana crystal-rich pumice as parent and the least evolved Toconao pumice as daughter, and employs the mineral compositions observed in the Atana pumice. The best-fit fractionating assemblage (smallest residual) from this analysis was then used to model selected trace element abundances by Rayleigh fractionation. We chose to model only the three elements

Rb, Ba and Sr, whose abundances can be reasonably assumed to be unaffected by accessory mineral fractionation. Fractional crystallization can be accepted as a viable process if both major and trace element variations can be modelled at a common value of F (proportion of residual liquid). Partition coefficients (K_D values) for Ba, Sr and Rb in plagioclase and hornblende and for Ba in biotite in dacites represent values measured by Schmitt (1999) in an SIMS study of the Purico dacite, an APVC unit similar in composition to the Atana dacite. These K_D values fall within the published range for these minerals in other dacites and rhyolites. Remaining K_D values for modelled minerals in dacites and rhyolites were selected from the literature (see Table 8 for references).

The least-squares model indicates that Toconao and Atana pumices can be related to each other by 30% fractional crystallization ($F = 0{\cdot}69$) of an assemblage containing 58% plagioclase (An_{68}), 21% biotite, 11% quartz, 5% hornblende, 4% magnetite, 1% apatite and 0·4% titanite (Table 8, part A). This mineral assemblage is similar to that actually observed in the Atana pumices (Table 1).

The trace element modelling yields F values of 0·69 and 0·66 for Sr and Rb, respectively, which agree well with the major element model. For Ba, however, the model yielded an F value of unity, reflecting the very small difference in Ba composition between the selected parent and daughter. Because of the large range in Ba compositions in the Toconao pumice population (200–700 ppm; Fig. 7b), modelling of this element is highly dependent on choice of daughter composition. Fractionation of the Atana magma by 30% crystallization of the model assemblage results in a Ba content in the residual magma of $\sim$350 ppm, well within the range observed for the Toconao pumices.

The variations in most other trace elements, such as Zr and the REE, cannot be modelled by this approach as they are essential components in accessory minerals. For example, removal of just 0·02% zircon is sufficient to bridge the compositional gap in Zr contents between the Atana and Toconao pumices (Fig. 10). The LREE depletion in the Toconao pumices relative to the Atana pumices (Fig. 8) can be explained qualitatively by fractionation of allanite and/or monazite, which are present in the pumice (Table 1) and which both have very high K_D values for the LREEs [up to 10^3–10^4, according to Miller & Mittlefehldt (1982)].

If, as we propose, the grey pumice inclusions represent crystal accumulations resulting from this fractionation process, then they should have a mineral assemblage similar to that predicted in the model. The mineral assemblage in the grey pumice inclusions comprises 60–63% plagioclase, 9–28% hornblende, 8–22% biotite, 2–4% Fe–Ti oxides, 0–4% clinopyroxene, with traces of orthopyroxene, titanite, zircon and apatite. Apart from quartz, this is consistent with the model assemblage (Table 8, part A). The mineral compositions are also consistent: the model plagioclase composition for example is An_{68}, which lies near the middle of the grey inclusion range. The only inconsistency with the model is that quartz is not present in the grey pumice inclusions. The absence of quartz, which is likely to crystallize at more advanced stages of fractionation, can be reconciled if the inclusions comprise crystals formed early in the fractionation process at the side-walls of the magma chamber as proposed by de Silva (1989*c*).

One remaining problem with this model concerns the difference in H_2O content between the Toconao and Atana ignimbrites. The removal of 30% anhydrous and hydrous minerals in the model assemblage would lead to an H_2O increase of $\sim$1 wt % in the daughter melt. This represents at best only half of the difference observed between the Atana and Toconao melts. This implies either that further fractionation of the Toconao magma occurred, as is suggested by the range in pumice compositions (Fig. 7), or that processes other than crystal–melt fractionation operated to increase H_2O to the calculated 6 wt %. One possibility would be diffusive transport of dissolved H_2O upward in the magma.

Compositional variation within the Toconao ignimbrite

Toconao pumices show a large compositional range for some elements and a correlation of composition with location relative to the caldera. Pumice clasts from the east and southwest of the caldera generally display a greater range and more evolved compositions than those from the west. In these eastern and southwestern localities, the Toconao ignimbrite lacks the vapour-phase altered facies, and both tube and crystal-poor pumices are present. These differences in pumice type and composition may imply different eruption pulses, with the more evolved, eastern and southwestern samples perhaps representing an earlier pulse. It can be speculated that the first erupted, more evolved magma would have been more water rich, and therefore less viscous, conditions that may have impeded the formation of tube pumices.

The large range in trace element concentrations for a correspondingly very small variation in major elements (i.e. <2 wt % SiO_2) is a common feature of high-Si rhyolites such as the Toconao ignimbrite. Table 8, part B, shows an attempt to model the trace element variation within the Toconao pumice population by Rayleigh fractionation. Calculations were carried out using modal mineral proportions observed in the Toconao pumices, and parent and daughter compositions selected from the lowest and highest end of the compositional range for the incompatible element Rb. Solving the Rayleigh fractionation equation for Rb, Ba and Sr reveals similar F values of 0·84, 0·91 and 0·94, indicating that only minor

Table 8: Fractional crystallization models

A: Atana most evolved pumice to Toconao least evolved pumice

Element	Daughter Toc-97h-3	Plag 58%	Hbl 4·8%	Bt 21%	Mt 3·5%	Titn 0·4%	Qtz 11·3%	Ap 1%	Parent Lari-96h-4	Parent (calc) $F = 0.69$	Difference r^2
SiO_2	76·7	51·6	46·0	37·5	0·1	29·6	100·0	—	68·9	68·9	0·00
TiO_2	0·12	—	1·59	4·74	5·14	35·56	—	—	0·52	0·54	−0·02
Al_2O_3	12·9	31·0	8·0	13·7	1·4	1·5	—	—	15·5	15·5	−0·01
FeO_t	0·63	0·27	15·18	17·51	85·14	1·88	—	—	2·91	2·91	0·00
MnO	0·07	—	0·43	0·25	0·59	0·09	—	—	0·06	0·08	−0·02
MgO	0·08	—	13·05	13·28	0·59	—	—	—	1·14	1·16	−0·01
CaO	0·61	14·04	11·61	0·02	0·01	26·44	—	55·00	3·36	3·34	0·02
Na_2O	3·97	3·58	1·45	0·37	—	0·03	—	—	3·40	3·43	−0·03
K_2O	4·88	0·19	0·90	8·79	—	0·02	—	—	4·04	4·01	0·04
P_2O_5	0·02	—	—	—	—	—	—	45·00	0·13	0·16	−0·03
Sum	100	100·62	98·23	96·93	98·79	95·09	100·00	100·00	100	100	0·00
	ppm	K_D values							*ppm*	Bulk *D*	*F*
Ba	598	0·70[1]	0·50[1]	16·90[1]	0·10[3]	0·00	0·02[4]	0·45[5]	575	3·96	1·01
Sr	53	9·00[1]	0·94[1]	0·12[2]	0·08[2]	0·00	0·00[4]	2·10[5]	260	5·32	0·69
Rb	220	0·04[1]	0·09[1]	2·24[2]	0·01[2]	0·00	0·04[4]	0·40[5]	179	0·50	0·66

B: Toconao least evolved to most evolved pumice

Element	Daughter Quis-96h-4a (ppm)	K_D values Plag 62%	Bt 2%	Sa 24%	Qtz 12%	Parent Toc-97h-3 (ppm)	Bulk *D*	*F*
Ba	441	1·52[2]	7·00[4]	11·45[2]	0·00	598	3·83	0·91
Sr	34	8·00[2]	0·45[4]	2·00[2]	0·00	53	5·45	0·94
Rb	256	0·11[2]	2·30[4]	0·11[2]	0·00	220	0·14	0·84

The mineral compositions used for hornblende, biotite, magnetite and titanite are average core compositions of these minerals in the Atana pumice. The plagioclase composition of An_{68} required by the model represents a typical core spot analysis towards the mafic end of the Atana pumice range (see Fig. 5). Magnetite sums are based on the analysis after recalculation of ferric and ferrous Fe [following Droop (1987)]. Biotite sums include BaO, F and Cl (not presented). The sum in the 'difference' (r^2) column refers to the sum of squares of differences. K_D values from: [1]Schmitt (1999); [2]Ewart & Griffin (1994); [3]Bacon & Druitt (1988); [4]Nash & Crecraft (1985); [5]Mahood & Stimac (1990).

crystallization (6–16%) is required to explain their compositional range. The fanning out of the LREE patterns within the Toconao pumice population (Fig. 8) is consistent with slight variations in monazite and/or allanite content. Accessory mineral fractionation may have therefore played an important role in generating the observed compositional variation for the LREE.

Problems with modelling the Toconao magma are that the pumice clasts are largely aphyric, making it difficult to choose realistic mineral proportions, and that published K_D values for high-Si rhyolites are highly variable. Considering these uncertainties, the results must be considered qualitative and we conclude that the variation in Toconao pumice chemistry is consistent with fractional crystallization of observed mineral phases. This agrees with other studies (e.g. Miller & Mittlefehldt, 1984; Streck & Grunder, 1997) where extreme trace element gradients in high-Si rhyolites were attributed to fractionation of

minimum melt compositions in compositionally stratified magma chambers.

The only inconsistency with closed-system fractional crystallization as a process generating the Toconao pumice compositional variation is the considerable range in ε_{Nd} and $^{87}Sr/^{86}Sr_i$ (Fig. 9, inset). This range indicates that a strictly closed-system fractionation model is too simple to explain the variation in composition in the Toconao pumice population. We suggest that some assimilation, perhaps by roof-rock contamination as proposed by Duffield *et al.* (1995) for the Bishop Tuff, may have played a role in the evolution of the Toconao magma.

A magma chamber model

The geochemical and petrological evidence shows that the Toconao and Atana magmas are cogenetic, and can be related to each other by crystal fractionation. A physical model of crystal–liquid fractionation in the La Pacana magma chamber must be able to explain the extremely crystal-poor nature of the Toconao ignimbrite and its considerable volume: the Toconao and Atana outflow tuffs are more or less the same size ($\sim$200 km^3; Lindsay *et al.*, 2001). It must also explain the homogeneity of the Atana ignimbrite and the presence of grey, crystal-rich pumice inclusions. The simplest model that accounts for all these features is one in which crystals and melt separate from a convecting Atana magma by density differences, resulting in a stratified magma chamber with a homogeneous central zone, a crystal-rich accumulation zone near the walls or base, and a buoyant, melt-rich zone near the top. This is consistent with the estimated magma temperatures and densities: the pre-eruptive Toconao magma was cooler (740°C) and more volatile rich (6 wt % H_2O) than the Atana magma (780°C; 2–3 wt % H_2O), and its density was lower (2·25 g/cm^3 vs 2·50 g/cm^3). Evidence for convection in the Atana magma is provided by the remarkable mineralogical and chemical homogeneity of the Atana crystal-rich pumices, which show no significant variation with height in the flow unit or distance from source.

It has been suggested that magma chamber shape plays an important role in determining the effectiveness of side-wall convective fractionation vs differentiation by crystal settling in magma chambers (de Silva & Wolff, 1995). Large-volume, homogeneous ignimbrites such as the Atana ignimbrite are thought to erupt from magma chambers with high aspect ratios (i.e. sill-shaped), in which side-wall crystallization is considered ineffective, and significant zonation is not produced because crystallization proceeds mainly in the main part of the convecting magma (Martin & Nokes, 1988, 1989; de Silva & Wolff, 1995).

A schematic model for the La Pacana magma chamber that takes into consideration these arguments is presented in Fig. 12. Fractionation of the convecting dacitic magma in a sill-like chamber led to the generation of a zone of buoyant melt at the top of the chamber, perhaps in a cupola. According to Marsh (1981), constraints from crystal packing make melt extraction possible until crystallization exceeds 50–60%. This evolved residual melt was effectively separated from the convecting dacitic magma by density differences. Continued differentiation in the cupola by side-wall fractionation may have produced the zonation observed in the Toconao magma. The Toconao magma did not mix with the Atana magma during eruption, implying that it was too thick, or the discharge rate too low, for the critical draw-down depth to reach the Atana magma below. The relationship between discharge rate and draw-down depth can be estimated by the method of Blake & Ivey (1986). Eruption rates of the Toconao ignimbrite are unknown but assuming rates typical of ignimbrite eruptions (10^4–10^5 m^3/s), a thickness of at least 200–300 m for the Toconao magma is required to prevent draw-down reaching the Atana magma beneath.

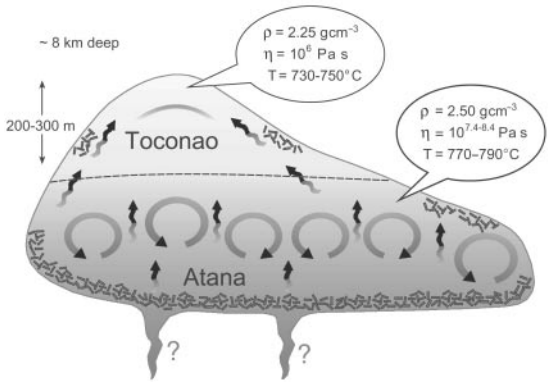

Fig. 12. Schematic model of the La Pacana magma chamber based on inferred pre-eruptive conditions. Fractionation of the convecting Atana magma, primarily by crystal settling, leads to the development of a buoyant, volatile-rich, evolved melt that ponds at the top of the magma chamber. These two magmas remain separated because of density differences. Crystallization from the volatile-rich differentiate, primarily at the side-walls, leads to further fractionation and zoning within this high-Si Toconao magma. Wavy arrows indicate movement of differentiated melt.

Eruption triggers

Differences in pumice-type, pre-eruptive H_2O contents and temperatures of the Toconao and Atana ignimbrites, along with the presence of a plinian deposit at the base of the Toconao but not the Atana, may indicate different eruption triggers for these two units. Toconao tube pumices reflect eruption of a relatively viscous, volatile-rich, almost aphyric magma, whereas the Atana crystal-rich pumices reflect eruption of dense, viscous, relatively volatile-poor, crystal-rich magma.

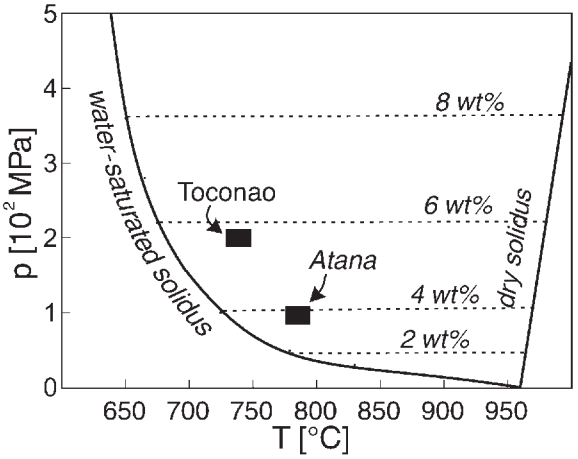

Fig. 13. Water saturation curves for haplogranitic melts after Holtz & Johannes (1994) compared with estimated pre-eruptive temperatures and pressures for the Atana and Toconao melts. At a pressure of 200 MPa, the Toconao melt with its 6 wt % H_2O is water saturated; the Atana melt, with 3–4 wt % H_2O, is not.

Ignimbrite-producing magmas are commonly thought to erupt when volatile exsolution proceeds to a degree such that magma strain rate overcomes magma relaxation time and explosive fragmentation occurs (Dingwell, 1996; Papale, 1999). For this to happen, a magma must be oversaturated in volatiles (especially H_2O) at pre-eruptive pressures and temperatures, such that an overpressure in the magma chamber can develop. We tested this condition by comparing the pre-eruptive temperatures (740 and 780°C) and pressures (200 MPa) for the Toconao and Atana melts with experimentally determined water saturation curves for haplogranitic melts from Holtz & Johannes (1994), in Fig. 13. The experimental curves suggest that 5–6 wt % H_2O would be required for water saturation at the inferred conditions of the Toconao and Atana melts. The Toconao melt, with 6 wt % H_2O, could have vesiculated at this depth, thus increasing internal pressure and magma strain rate, inducing fragmentation and eruption. This is consistent with the presence of the small plinian deposit at the base of the Toconao ignimbrite. On the other hand, the Atana melt water contents were 3–4 wt %, too low for vesiculation in the magma at 200 MPa. The experimental curves in Fig. 13 show that H_2O saturation and exsolution in the Atana magma, with melt H_2O contents of 3–4 wt %, would occur if confining pressure were reduced to 100 MPa. The high viscosity and crystallinity and low H_2O content of the Atana should prohibit it erupting as an ignimbrite, according to the empirical model of Scaillet *et al.* (1998). Thus a mechanism is required to either increase internal magma pressure or reduce confining pressure.

One mechanism of increasing internal magma pressure is by recharge of basic magma, which leads to an increase in both volume and volatiles in the felsic chamber. The homogeneity of the Atana magma has already been stressed, and no quenched mafic inclusions have been found that would give evidence for recharge of a more basic magma before eruption.

A reduction in confining pressure would occur by disruption of the roof rocks, and an obvious mechanism for achieving this is through the precursor eruption of the Toconao ignimbrite. In addition, the evidence for tectonic control on the caldera collapse is compelling: (1) La Pacana has a half-graben geometry and the distribution of the Atana ignimbrite suggests a trap-door-like collapse (Lindsay *et al.*, 2001); (2) eruptive transport of the magma to the surface appears to have been rapid, as there are no reaction rims on hornblende: experiments on dacites by Rutherford & Hill (1993) indicate that hornblende in contact with melt develops reaction rims within 4–20 days of decompression; (3) the lack of a plinian deposit associated with the Atana ignimbrite implies an instantly collapsing eruption column, which in turn suggests a large conduit; (4) a number of regional faults pass through La Pacana caldera, the largest of which is the NW–SE trending Calama–Olacopato–El Toro lineament (Fig. 1). All of these observations are consistent with the hypothesis of an external, tectonic trigger for the eruption of the Atana magma, with or without weakening of the roof rocks as a result of the Toconao eruption.

The inferred presence of an evolved cap of volatile-rich, crystal-poor melt in the La Pacana magma chamber shows that large-volume, crystal-rich dacitic magmas can significantly fractionate and develop a zoned magma chamber, yet maintain their homogeneous character. Other large-volume, crystal-rich, intermediate-composition ignimbrites of the world (e.g. Galán Ignimbrite, Francis *et al.*, 1989; Fish Canyon Tuff, Lipman *et al.*, 1978; Whitney & Stormer, 1985; Monotony Tuffs, Best *et al.*, 1989, 1995) do not appear to be associated with underlying, crystal-poor, rhyolite tuffs. The Atana ignimbrite is very similar to these 'monotonous intermediates', yet shows evidence for a felsic cap. The reason for this may be related to their eruption trigger: if crystal-rich, dacitic magma chambers experienced significant recharge or a tectonic event early in their evolution, eruption may be triggered before significant production of rhyolitic differentiates such as the Toconao ignimbrite.

Many crystal-poor, rhyolitic tuffs in the APVC are not associated with crystal-rich, dacitic ignimbrites of similar age (e.g. Pampa Chamaca, Talabre, Patao, Caspana, Yerbas Buenas, Carcoté ignimbrites). These rhyolites are generally smaller in volume than the Toconao ignimbrite, and could come from smaller systems as proposed by de Silva (1991) and Siebel *et al.* (2000). Alternatively, these ignimbrites may represent a portion of the evolved cap

of a zoned system, in which the dacitic 'Atana equivalent' remains unerupted. This is consistent with the interpretation that the crystal-rich, dacitic Atana magma would have failed to erupt if eruption had not been triggered externally.

Source constraints for the La Pacana magma

The Atana ignimbrite is typical of many large-volume, crystal-rich ash flow tuff units in the APVC and information gained in this study can therefore be used to test and refine existing models for the generation of this important magma type. The consistency in physical and geochemical characteristics of these ignimbrites was interpreted by de Silva (1989*a*) to indicate a regionally consistent process of magma generation. He noted the correspondence between the timing of ignimbrite 'flare-up' at ~10 Ma with crustal thickening in the Central Volcanic Zone (CVZ) and with a period of high convergence rate between the South American and Nazca plates. The increased flux of subduction-related magma, coupled with a thicker crust, was suggested to create conditions favourable for crustal melting. This concept is supported by modelling of Laube & Springer (1998), who explored the thermal consequences of arc andesite magmas being ponded in the mid-crust and showed that the input of heat and magmatic volatiles could cause crustal melting on the scale required for the APVC ignimbrite magmatism.

The large-volume ignimbrites in the APVC and Cerro Galan (Fig. 1) have long been considered to have a crustal source based on their radiogenic isotopic compositions (e.g. de Silva, 1989*a*; Francis & Hawkesworth, 1994). Our Sr and Nd isotopic data (Fig. 9) show that the Atana and Toconao ignimbrites share these characteristics and are isotopically distinct from coeval arc stratovolcanoes in the CVZ, which themselves have undergone considerable crustal contamination (Davidson *et al.*, 1990; Trumbull *et al.*, 1999). The Sr and Nd isotopic ratios are comparatively sensitive to mixing of crustal and mantle-derived magmas because the concentrations of Sr and Nd in both components are similar. This is not the case for Pb isotopes, because of the very low Pb concentration in mantle-derived magmas compared with the continental crust. Therefore, the Pb isotope ratios of hybrid magmas should be dominated by the signature of the crustal component. The Pb isotope ratios of La Pacana ignimbrites show little variation, with $^{206}Pb/^{204}Pb$ and $^{208}Pb/^{204}Pb$ values of 18·91–19·00 and 38·06–39·15, respectively. These values are similar to those reported from the Panizos (Ort *et al.*, 1996) and Galan ignimbrites (Francis *et al.*, 1989), and they correspond to the Southern Altiplano basement domain defined from Pb isotopes by Aitcheson *et al.* (1995).

Identification of the crustal material involved in the La Pacana magma source and the proportion of crustal to mantle-derived material is extremely difficult because of the heterogeneity of pre-Andean basement. The metaluminous to weakly peraluminous bulk composition of the La Pacana ignimbrites rules out an important role of metapelitic rocks in the crustal source, as was argued for the peraluminous Macusani ignimbrites in southern Peru (Pichavant *et al.*, 1988). The basement field plotted in Fig. 9 includes quartzo-feldspathic metaluminous gneisses and granitoids from the APVC region [Lucassen *et al.* (1999) and references therein], and these are likely candidates for the crustal source. This does not imply that the La Pacana ignimbrites derive from purely crustal melts. Indeed, if the crustal source is similar to the Palaeozoic gneisses and granitoids at present exposed, the ignimbrites cannot represent pure crustal melts. Dehydration melting experiments (e.g. Patiño-Douce, 1996; Castro *et al.*, 1999) show that biotite-bearing felsic protoliths yield highly silicic, iron- and magnesium-poor, peraluminous compositions that do not match those of the large-volume dacitic ignimbrites. Experimental melting of quartz amphibolite yielded high-Si melts that also differ greatly from the compositions observed in the APVC. Furthermore, if the ignimbrites are products of either bulk or partial melting of Palaeozoic felsic crust, their moderately radiogenic $^{87}Sr/^{86}Sr$ ratios (0·7094–0·7131) demand a low time-integrated Rb/Sr ratio in the source. This is not entirely consistent with the exposed basement compositions and it is difficult to imagine a source rich enough in biotite to generate abundant dehydration melts and at the same time having a low bulk Rb/Sr ratio. Therefore we suggest that the ignimbrite source magmas are hybrids. The considerable range in Sr isotopic ratios in both the Toconao and Atana ignimbrites probably reflects incomplete homogenization of isotopic heterogeneity generated from partial melting of a heterogeneous crust with an admixture of mantle-derived melts. Modelling the proportions of crustal and mantle-derived materials in the La Pacana source magmas is not attempted because of the variation in basement data and almost total lack of information on the deeper crust. Ort *et al.* (1996) suggested that the proportion of mantle-derived material in the source of the Panizos ignimbrite was as much as 50%.

There are no resorbed xenoliths or other clear petrographic evidence in the Atana samples for interaction with upper crust at the level of the La Pacana magma chamber (780°C at 7–9 km) and large-scale crustal melting at this level can be ruled out from thermal constraints (Laube & Springer, 1998; Springer, 1999). Therefore the intensive parameters determined in this study reflect mineral equilibration at the storage level of a magma that was sourced from deeper in the crust. The depth of crustal melting is elusive, but REE concentration ratios

in the erupted rocks (chondrite-normalized La/Yb ratios are 9–12) are not consistent with significant garnet in the source, which has high partition coefficients for the HREE. Patiño-Douce & Beard (1995) showed that garnet is produced in biotite and amphibole melting reactions in quartzo-feldspathic gneisses at pressures >1000 MPa, and this would suggest that the zone of melting is above ~30 km.

Support for the interpretation of large-scale melting in the mid-crust is given by a number of geophysical anomalies under the western Altiplano–Puna plateau, which suggest a zone of partial melting at ~20 km depth. Low seismic P- and S-wave velocities, high V_p/V_s ratios and high electrical conductivity have been interpreted to indicate the presence of partial melt (Schilling *et al.*, 1997; Schmitz *et al.*, 1997). Chmielowski *et al.* (1999) used seismic receiver function analysis to delineate a zone at 19 km under the APVC with extremely low S-wave velocities, which they also interpreted to indicate partial melting. This geophysical evidence therefore supports our petrological arguments, and suggests that conditions conducive to generation of a partially molten zone in the CVZ crust at 4 Ma persist to the present day.

CONCLUSIONS

The results of this geochemical and isotopic study of the ignimbrites associated with the La Pacana caldera system lead to the following conclusions:

(1) the crystal-rich dacitic Atana ignimbrite (2500 km^3) and the crystal-poor rhyolitic Toconao ignimbrite (200 km^3) represent cogenetic magmas. Evidence for this is their similar geological distribution, their overlapping ages, concordant isotopic compositions and the fact that Atana pumice glasses and rare crystal-poor rhyolite pumices in the Atana ignimbrite are very similar in composition to typical Toconao tube pumices. The differences in major and trace element composition between typical Toconao pumice and Atana crystal-rich pumice can be explained by their different crystal contents. This is quantified by fractional crystallization modelling, which shows that the Toconao magma can be viewed as residual melt after 30% crystallization of the mineral assemblage observed in the Atana pumices.

(2) The composition of Toconao pumice and Atana rhyolitic pumice clasts reveals a large compositional range for many trace elements in the chemically evolved cap of the zoned pre-eruptive magma chamber. The Toconao data indicate that the greatest variation and the most evolved compositions are present in outflow ignimbrite from the east and southwest of the caldera. This is interpreted as reflecting zoning in the magma, whereby the eastern and southwestern outflow may represent the earliest erupted (i.e. uppermost) portion of the chamber.

(3) Mineral thermobarometry shows that the pre-eruptive Atana magma equilibrated at temperatures between 770 and 790°C, and pressures between 190 and 230 MPa. Mineral barometers are lacking in Toconao pumice, but thermometry indicates that the pre-eruptive Toconao magma was somewhat cooler (730–750°C). Water contents of the Atana and Toconao magmas are estimated at 2–3 wt % and 6 wt %, respectively. Magmatic densities are lower in the Toconao (2·25 g/cm^3) than in the Atana (2·50 g/cm^3). These pre-eruptive conditions are consistent with the Toconao magma representing the evolved cap of the Atana magma chamber.

(4) H_2O contents in the Toconao magma are consistent with volatile exsolution triggering eruption at the inferred pre-eruptive pressure of ~200 MPa. The Atana magma, however, was not saturated in H_2O at 200 MPa. This, together with its high viscosity and crystal content, suggests that the Atana magma required an external trigger to erupt. Caldera geometry and association with regional faults suggests a tectonic influence, perhaps on roof rocks weakened by the Toconao eruption.

(5) The similarity in geochemical and isotopic characteristics between the Atana and other large-volume, crystal-rich ignimbrites in the APVC implies a common petrogenesis; we agree with current models that invoke crustal melting as the predominant magma-generation process. Thermal constraints, together with a lack of chemical or petrographic evidence for interaction with upper crust at the level of the La Pacana magma chamber, rule out large-scale crustal melting at this depth (7–9 km). Petrological arguments imply a zone of melting above ~30 km. Geophysical anomalies beneath the western Altiplano–Puna plateau suggest a zone of partial melt at ~20 km depth, suggesting that conditions conducive to generation of a partially molten zone in the CVZ crust at 4 Ma persist to the present day.

ACKNOWLEDGEMENTS

This study was carried out as part of the special research centre SFB-267, 'Deformation processes in the Andes', funded by the Deutsche Forschungsgemeinschaft (DFG). Thanks are due to numerous colleagues in the SFB for their support, including many productive discussions. We would like to thank the staff at the Universidad Católica del Norte in Antofagasta, Chile, for logistical support in the field, and Moyra Gardeweg from the SERNAGEOMIN in Santiago for constructive discussions. Melt inclusion analyses were carried out at Arizona State University by A. Schmitt, who gratefully acknowledges financial support by the DAAD and the assistance of Rick Hervig, John Holloway and Ed Bailey at ASU. We are grateful to our Potsdam colleagues for support with analytical work, in particular Rudolf Naumann (XRF),

Hans-Gerrit Plessen (ICP-MS), Erika Kramer (ICP-AES) and Dieter Rhede (electron microprobe). We acknowledge the crucial contributions of Peter Francis and Steve Self to earlier studies of the La Pacana system. Finally, the thorough journal reviews by Anita Grunder, Michael Ort and Michael Dungan greatly improved the presentation of our results.

REFERENCES

Ahrens, T. A. (ed.) (1995). *Mineral Physics and Crystallography: a Handbook of Physical Constants 2*. Washington, DC: American Geophysical Union.

Aitcheson, S. J., Harmon, R. S., Moorbath, S., Schneider, A., Soler, P., Soria-Escalante, E., Steele, G., Swainbank, I. & Wörner, G. (1995). Pb isotopes define basement domains of the Altiplano, Central Andes. *Geology* **23**, 555–558.

Anders, E. & Grevesse, N. (1989). Abundances of the elements: meteoritic and solar. *Geochimica et Cosmochimica Acta* **53**, 197–214.

Andersen, D. J. & Lindsley, D. H. (1988). Internally consistent solution models for Fe–Mg–Mn–Ti oxides; Fe–Ti oxides. *American Mineralogist* **73**, 714–726.

Andersen, D. J., Lindsley, D. H. & Davidson, P. M. (1993). QUILF: a Pascal program to assess equilibria among Fe–Mg–Mn–Ti oxides, pyroxenes, olivine and quartz. *Computers and Geosciences* **19**, 1333–1350.

Anderson, J. L. & Smith, D. R. (1995). The effects of temperature and fO_2 on the Al-in-hornblende barometer. *American Mineralogist* **80**, 549–559.

Bacon, C. R. & Druitt, T. H. (1988). Compositional evolution of the zoned calcalkaline magma chamber of Mount Mazama, Crater Lake, Oregon. *Contributions to Mineralogy and Petrology* **98**, 224–256.

Bacon, C. R. & Hirschmann, M. M. (1988). Mg/Mn partitioning as a test for equilibrium between coexisting Fe–Ti oxides. *American Mineralogist* **73**, 57–61.

Beck, S. L., Zandt, G., Myers, S. C., Wallace, T. C., Silver, P. G. & Drake, L. (1996). Crustal thickness variations in the Central Andes. *Geology* **24**, 407–410.

Best, M. G., Christiansen, E. H., Deino, A. L., Gromme, C. S., McKee E. H. & Noble, D. C. (1989). Excursion 3A; Eocene through Miocene volcanism in the Great Basin of the Western United States. *New Mexico, Bureau of Mines and Mineral Resources Memoir* **47**, 91–133.

Best, M. G., Christiansen, E. H., Deino, A. L. & Gromme, C. S. (1995). The central Nevada caldera complex in the middle Tertiary ash-flow province of the Great Basin, USA. In: *International Union of Geodesy and Geophysics, General Assembly 21, Week A, Abstracts*. Boulder, CO: IUGS, 444 pp.

Blake, S. & Ivey, G. N. (1986). Magma-mixing and the dynamics of withdrawal from stratified reservoirs. *Journal of Volcanology and Geothermal Research* **27**, 153–178.

Branney, M. J. & Kokelaar, B. P. (1994). Volcanotectonic faulting, soft-state deformation and rheomorphism of tuffs during development of a a piecemeal caldera: English Lake District. *Geological Society of America Bulletin* **106**, 507–530.

Castro, A., Patiño-Douce, A. E., Corretgé, L. G., de la Rosa, J. D., El-Biad, M. & El-Hmidi, H. (1999). Origin of peraluminous granites and granodiorites, Iberian massif, Spain: an experimental test of granite petrogenesis. *Contributions to Mineralogy and Petrology* **135**, 255–276.

Chmielowski, J., Zandt, G. & Haberland, C. (1999). The central Andean Altiplano–Puna magmatic body. *Geophysical Research Letters* **26**, 783–786.

Christiansen, R. L. (1984). Yellowstone magmatic evolution: its bearing on understanding large-volume explosive volcanism. In: Boyd, F. R. (ed.) *Explosive Volcanism: Inception, Evolution and Hazards*. Washington, DC: National Academy Press, pp. 84–95.

Davidson, J. P., McMillan, N. J., Moorbath, S., Wörner, G., Harmon, R. S. & Lopez-Escobar, L. (1990). The Nevados de Payachata volcanic region (18°S, 69°W, N. Chile); II, Evidence for widespread crustal involvement in Andean magmatism. *Contributions to Mineralogy and Petrology* **105**, 412–432.

Deer, W. A., Howie, R. A. & Zussman, J. (1992). *An Introduction to the Rock-forming Minerals*, 2nd edn. Harlow, UK: Longman.

de Silva, S. L. (1989*a*). Altiplano–Puna volcanic complex of the central Andes. *Geology* **17**, 1102–1106.

de Silva, S. L. (1989*b*). Geochronology and stratigraphy of the ignimbrites from the 21°30′S to 23°30′S portion of the Central Andes of northern Chile. *Journal of Volcanology and Geothermal Research* **37**, 93–131.

de Silva, S. L. (1989*c*). The origin and significance of crystal rich inclusions in pumices from two Chilean ignimbrites. *Geological Magazine* **126**, 159–175.

de Silva, S. L. (1991). Styles of zoning in central Andean ignimbrites; insights into magma chamber processes. In: Harmon, S. R. & Rapela, C. W. (eds) *Andean Magmatism and its Tectonic Setting. Geological Society of America, Special Paper* **265**, 217–232.

de Silva, S. L. & Francis, P. W. (1989). Correlation of large ignimbrites; two case studies from the Central Andes of northern Chile. *Journal of Volcanology and Geothermal Research* **37**, 133–149.

de Silva, S. L. & Wolff, J. A. (1995). Zoned magma chambers; the influence of magma chamber geometry on sidewall convective fractionation. *Journal of Volcanology and Geothermal Research* **65**, 111–118.

Dingwell, D. B. (1996). Volcanic dilema; flow or blow? *Science* **273**(5278), 1054–1055.

Droop, G. T. R. (1987). A general equation for estimating Fe^{3+} concentrations in ferromagnesian silicates and oxides from microprobe analyses, using stoichiometric criteria. *Mineralogical Magazine* **51**, 431–435.

Duffield, W. A., Ruiz, J. & Webster, J. D. (1995). Roof-rock contamination of magma along the top of the reservoir for the Bishop Tuff. *Journal of Volcanology and Geothermal Research* **69**, 187–195.

Ewart, A. & Griffin, W. L. (1994). Application of proton-microprobe data to trace-element partitioning in volcanic rocks. *Chemical Geology* **117**, 251–284.

Francis, P. & Hawkesworth, C. (1994). Late Cenozoic rates of magmatic activity in the Central Andes and their relationships to continental crust formation and thickening. *Journal of the Geological Society, London* **151**, 845–854.

Francis, P. W., Sparks, R. S. J., Hawkesworth, C. J., Thorpe, R. S., Pyle, D. M., Tait, S. R., Mantovani, M. S. & McDermott, F. (1989). Petrology and geochemistry of volcanic rocks of the Cerro Galán caldera, northwest Argentina. *Geological Magazine* **126**, 515–547.

Fuhrman, M. L. & Lindsley, D. H. (1988). Ternary-feldspar modelling and thermometry. *American Mineralogist* **73**, 201–215.

Futa, K. & Stern, C. R. (1988). Sr and Nd isotopic and trace element compositions of Quaternary volcanic centers of the Southern Andes. *Earth and Planetary Science Letters* **88**, 253–262.

Gardeweg, M. & Ramírez, C. F. (1987). The La Pacana caldera and the Atana ignimbrite—a major ash-flow and resurgent caldera complex in the Andes of northern Chile. *Bulletin of Volcanology* **49**, 547–566.

Gerstenberger, H. & Haase, G. (1997). A highly effective emitter substance for mass spectrometric Pb isotope ratio determinations. *Chemical Geology* **136**, 309–312.

Ghiorso, M. S. (1984). Activity/composition relations in the ternary feldspars. *Contributions to Mineralogy and Petrology* **87**, 282–296.

Green, N. L. & Usdansky, S. I. (1986). Ternary-feldspar mixing relations and thermobarometry. *American Mineralogist* **71**(9–10), 1100–1108.

Guest, J. E. (1969). Upper Tertiary ignimbrites in the Andean cordillera of part of the Antofagasta Province, northern Chile. *Geological Society of America Bulletin* **80**, 337–362.

Hammarstrom, J. M. & Zen, E-An (1986). Aluminum in hornblende; an empirical igneous geobarometer. *American Mineralogist* **71**, 1297–1313.

Hildreth, W. & Moorbath, S. (1988). Crustal contributions to arc magmatism in the Andes of central Chile. *Contributions to Mineralogy and Petrology* **98**, 455–489.

Holland, T. & Blundy, J. (1994). Non-ideal interactions in calcic amphiboles and their bearing on amphibole–plagioclase thermometry. *Contributions to Mineralogy and Petrology* **116**, 433–447.

Holtz, F. & Johannes, W. (1994). Maximum and minimum water contents of granitic melts; implications for chemical and physical properties of ascending magmas. *Lithos* **32**, 149–159.

Houghton, B. F. & Wilson, C. J. N. (1989). A vesicularity index for pyroclastic deposits. *Bulletin of Volcanology* **51**, 451–462.

Housh, T. B. & Luhr, J. F. (1991). Plagioclase–melt equilibria in hydrous systems. *American Mineralogist* **76**, 477–492.

James, D. E. (1982). A combined O, Sr, Nd and Pb isotopic and trace element study of crustal contamination in central Andean lavas, I. Local geochemical variation. *Earth and Planetary Science Letters* **57**, 47–62.

Johnson, M. C. & Rutherford, M. J. (1989). Experimental calibration of the aluminum-in-hornblende geobarometer with application to Long Valley Caldera (California) volcanic rocks. *Geology* **17**, 837–841.

Kokelaar, B. P. (1992). Ordovician marine volcanic and sedimentary record of rifting and volcanotectonism: Snowdon, Wales, U.K. *Geological Society of America Bulletin* **104**, 1433–1455.

Kroll, H., Evangelakakis, C. & Voll, G. (1993). Two-feldspar geothermometry; a review and revision for slowly cooled rocks. *Contributions to Mineralogy and Petrology* **114**, 510–518.

Lange, R. A. (1994). The effect of H_2O, CO_2 and F on the density and viscosity of silicate melts. In: Carroll, M. R. & Holloway, J. R. (eds) *Volatiles in Magmas. Mineralogical Society of America, Reviews in Mineralogy* **30**, 331–369.

Laube, N. & Springer, J. (1998). Crustal melting by ponding of mafic magmas: a numerical model. *Journal of Volcanology and Geothermal Research* **81**, 19–35.

Le Maitre, R. W. (ed.) (1989). *A Classification of Igneous Rocks and Glossary of Terms*. Oxford: Blackwell.

Lindsay, J. M. (1999). Stratigraphy, age relations and magmatic evolution of large-volume felsic ignimbrites of the La Pacana Caldera, Central Andes, Chile. *Scientific Technical Report STR99/16*. Potsdam: GeoForschungsZentrum Potsdam.

Lindsay, J., de Silva, S., Trumbull, R., Emmermann, R. & Wemmer, K. (2001). The La Pacana Caldera, N. Chile: a re-evaluation of one of the world's largest resurgent calderas. *Journal of Volcanology and Geothermal Research* (in press).

Lipman, P. W., Doe, B. R., Hedge, C. E. & Steven, T. A. (1978). Petrologic evolution of the San Juan volcanic field, southwestern Colorado; Pb and Sr isotope evidence. *Geological Society of America Bulletin* **89**, 59–82.

López-Escobar, L., Tagiri, M. & Vergara, M. (1991). Geochemical features of Southern Andes Quaternary Volcanics between 41°50′ and 43°00′S. In: Harmon, S. R. & Rapela, C. W. (eds) *Andean Magmatism and its Tectonic Setting. Geological Society of America, Special Paper* **265**, 45–56.

Lucassen, F., Franz, G., Thirlwall, M. F. & Mezger, K. (1999). Crustal recycling of metamorphic basement: Late Palaeozoic granitoids of northern Chile (22°S). Implications for the composition of the Andean crust. *Journal of Petrology* **40**, 1527–1551.

Mahood, G. A. & Stimac, J. A. (1990). Trace-element partitioning in pantellerites and trachytes. *Geochimica et Cosmochimica Acta* **54**, 2257–2276.

Marsh, B. D. (1981). On the crystallinity, probability of occurrence, and rheology of lava and magma. *Contributions to Mineralogy and Petrology* **78**, 85–98.

Martin, D. & Nokes, R. (1988). Crystal settling in a vigorously convecting magma chamber. *Nature* **332**, 534–536.

Martin, D. & Nokes, R. (1989). A fluid-dynamical study of crystal settling in convecting magmas. *Journal of Petrology* **30**, 1471–1500.

Miller, C. F. & Mittlefehldt, D. W. (1982). Depletion of light rare-earth elements in felsic magmas. *Geology* **10**, 129–133.

Miller, C. F. & Mittlefehldt, D. W. (1984). Extreme fractionation in felsic magma chambers, a product of liquid-state diffusion or fractional crystallization? *Earth and Planetary Science Letters* **68**, 151–158.

Moore, I. & Kokelaar, B. P. (1998). Tectonically controlled piecemeal caldera collapse: a case study of Glencoe volcano, Scotland. *Geological Society of America Bulletin* **110**, 1448–1466.

Nash, W. P. & Crecraft, H. R. (1985). Partition coefficients for trace elements in silicic magmas. *Geochimica et Cosmochimica Acta* **49**, 2309–2322.

Ort, M. H., Coira, B. L. & Mazzoni, M. M. (1996). Generation of a crust–mantle magma mixture: magma sources and contamination at Cerro Panizos, Central Andes. *Contributions to Mineralogy and Petrology* **123**, 308–322.

Papale, P. (1999). Strain-induced magma fragmentation in explosive eruptions. *Nature* **397**(6718), 425–428.

Patiño-Douce, A. E. (1996). Effects of pressure and water contents on the compositions of primary crustal melts. *Transactions, Royal Society of Edinburgh, Earth Sciences* **87**, 11–21.

Patiño-Douce, A. E. & Beard, J. S. (1995). Dehydration-melting of biotite gneiss and quartz amphibolite from 3 to 15 kbar. *Journal of Petrology* **36**, 707–738.

Pichavant, M., Kontak, D. J., Briqueu, L., Valencia, H. J. & Clark, A. H. (1988). The Miocene–Pliocene Macusani Volcanics, SE Peru; 2: Geochemistry and origin of a felsic peraluminous magma. *Contributions to Mineralogy and Petrology* **100**, 325–338.

Pichler, H. & Zeil, W. (1972). The Cenozoic rhyolite–andesite association of the Chilean Andes. *Bulletin Volcanologique* **35**, 424–452.

Pinkerton, H. & Stevenson, R. J. (1992). Methods of determining the rheological properties of magmas at sub-liquidus temperatures. *Journal of Volcanology and Geothermal Research* **53**, 47–66.

Pouchou, J. L. & Pichoir, F. (1984). Un nouveau modèle de calcul pour la microanalyse quantitative par spectrométrie de rayons x. *La Recherche Aérospatiale* **3**, 167–192.

Rogers, G. & Hawkesworth, C. J. (1989). A geochemical traverse across the north Chilean Andes: evidence for crust generation from the mantle wedge. *Earth and Planetary Science Letters* **91**, 271–285.

Rutherford, M. J. & Hill, P. M. (1993). Magma ascent rates from amphibole breakdown; an experimental study applied to the 1980–1986 Mount St. Helens eruptions. *Journal of Geophysical Research* **98**, 19667–19685.

Salfity, J. A. (1985). Lineamentos transversales al rumbo andino en el noroeste Argentino. *IV Congreso Geologico Chileno*. Antofagasta: Sociedad Geologica de Chile, 2-119–2-137.

Sanders, C. O. (1984). Location and configuration of magma bodies beneath Long Valley, California, determined from anomalous earthquake signals. *Journal of Geophysical Research* **89**, 8287–8302.

Scaillet, B., Holtz, F. & Pichavant, M. (1998). Phase equilibrium constraints on the viscosity of silicic magmas 1. Volcanic–plutonic comparison. *Journal of Geophysical Research* **103**, 27257–27266.

Schilling, F. R., Partzsch, G. M., Brasse, H. & Schwarz, G. (1997). Partial melting below the magmatic arc in the central Andes deduced from geoelectromagnetic field experiments and laboratory data. *Physics of the Earth and Planetary Interiors* **103**, 17–32.

Schmitt, A. K. (1999). Melt generation and magma chamber processes in the Purico Complex and implications for ignimbrite formation in the Central Andes. *Scientific Technical Report STR99/19*. Potsdam: GeoForschungsZentrum Potsdam.

Schmitz, M., Heinsohn, W. D. & Schilling, F. R. (1997). Seismic, gravity and petrologic evidence for partial melt beneath the thickened Central Andean crust (21–23°S). *Tectonophysics* **270**, 313–326.

Siebel, W., Schnurr, W. B. W., Hahne, K., Kraemer, B., Trumbull, R. B., van den Bogaard, P. & Emmermann, R. (2000). Geochemistry and isotope systematics of small- to medium-volume Neogene–Quaternary ignimbrites in the southern central Andes: evidence for derivation from andesitic magma sources. *Chemical Geology* **171**, 213–237.

Smith, R. B. & Braile, L. W. (1983). Crustal structure and evolution of an explosive silicic volcanic system at Yellowstone National Park. In: Boyd, F. R. (ed.) *Explosive Volcanism: Inception, Evolution and Hazards*. Washington, DC: National Academy Press, pp. 96–109.

Smith, R. D., Cameron, K. L., McDowell, F. W., Niemeyer, S. & Sampson, D. E. (1996). Generation of voluminous silicic magmas and formation of mid-Cenozoic crust beneath north–central Mexico: evidence from ignimbrites, associated lavas, deep crustal granulites, and mantle pyroxenites. *Contributions to Mineralogy and Petrology* **123**, 375–389.

Smith, R. L. (1960). Ash flows. *Geological Society of America Bulletin* **71**, 795–842.

Smith, R. L. & Bailey, R. A. (1966). The Bandelier Tuff; a study of ash-flow eruption cycles from zoned magma chambers. *Bulletin of Volcanology* **29**, 83–103.

Springer, M. (1999). Interpretation of heat-flow density in the Central Andes. *Tectonophysics* **306**, 377–395.

Streck, M. J. & Grunder, A. L. (1997). Compositional gradients and gaps in high-silica rhyolites of the Rattlesnake Tuff, Oregon. *Journal of Petrology* **38**, 133–163.

Tormey, D. R., Hickey-Vargas, R., Frey, R. A. & López-Escobar, L. (1991). Recent lavas from the Andean volcanic front (33–42°S); interpretations of along-arc compositional variations. In: Harmon, S. R. & Rapela, C. W. (eds) *Andean Magmatism and its Tectonic Setting. Geological Society of America, Special Paper* **265**, 57–77.

Trumbull, R. B., Wittenbrink, R., Hahne, K., Emmermann, R., Büsch, W., Gerstenberger, H. & Siebel, W. (1999). Evidence for Late Miocene to Recent contamination of arc andesites by crustal melts in the Chilean Andes (25–26°S) and its geodynamic implications. *Journal of South American Earth Sciences* **12**, 135–155.

Watson, E. B. & Harrison, T. M. (1983). Zircon saturation revisited: temperatures and compositional effects in a variety of crustal magma types. *Earth and Planetary Science Letters* **64**, 295–304.

Westrich, H. R. (1987). Determination of water in volcanic glasses by Karl–Fischer titration. *Chemical Geology* **63**, 335–340.

Whitney, J. A. & Stormer, J. C., Jr (1985). Mineralogy, petrology, and magmatic conditions from the Fish Canyon Tuff, central San Juan Volcanic Field, Colorado. *Journal of Petrology* **26**, 726–762.

Wigger, P. J., Schmitz, M., Araneda, M., Asch, G., Baldzuhn, S., Giese, P., Heinsohn, W.-D., Martinez, E., Ricaldi, E., Röwer, R. & Viramonte, J. (1994). Variation of the crustal structure of the Southern Central Andes deduced from seismic refraction investigations. In: Reutter, K.-J., Scheuber, E. & Wigger, P. J. (eds) *Tectonics of the Southern Central Andes*. Berlin: Springer, pp. 23–48.

Zandt, G., Velasco, A. A. & Beck, S. L. (1994). Composition and thickness of the southern Altiplano crust, Bolivia. *Geology* **22**, 1003–1006.

Zartman, R. E. & Haines, S. M. (1988). The plumbotectonic model for Pb isotopic systematics among major terrestrial reservoirs—a case for bi-directional transport. *Geochimica et Cosmochimica Acta* **52**, 1327–1339.

Zuleger, E. & Erzinger, J. (1988). Determination of the REE and Y in silicate materials with ICP-AES. *Fresenius Zeitschrift für Analytische Chemie* **232**, 140–143.